Journal of Mathematical Imaging and Vision 21: 53–80, 2004

On the Choice of Band-Pass Quadrature Filters

DJAMAL BOUKERROUI
Medical Vision Laboratory, Department of Engineering Science, University of Oxford, Parks Road, Oxford OX1 3PJ, UK; HEUDIASYC, UMR CNRS 65999, Université de Technologie de Compiègne, BP 20529-60205 Compiègne Cedex, France
djamal.boukerroui@hds.utc.fr

J. ALISON NOBLE AND MICHAEL BRADY
Medical Vision Laboratory, Department of Engineering Science, University of Oxford, Parks Road, Oxford OX1 3PJ, UK
noble@robots.ox.ac.uk
jmb@robots.ox.ac.uk

Abstract. Band-pass quadrature filters are extensively used in computer vision to estimate information from images such as: phase, energy, frequency and orientation,[1] possibly at different scales and utilise this in further processing-tasks. The estimation is intrinsically noisy and depends critically on the choice of the quadrature filters. In this paper, we first study the mathematical properties of the quadrature filter pairs most commonly seen in the literature and then consider some new pairs derived from the classical feature detection literature. In the case of feature detection, we present the first attempt to design a quadrature pair based on filters derived for optimal edge/line detection. A comparison of the filters is presented in terms of feature detection performance, wherever possible, in the sense of Canny and in terms of phase stability. We conclude with remarks on how our analysis can aid in the choice of a filter pair for a given image processing task.

Keywords: phase information, quadrature filter, feature detection, monogenic signal

1. Introduction

In computer vision and image analysis, arguably the most classical processing tools are amplitude-based techniques, both in the spatial and frequency domains. Consequently, throughout the history of digital image processing, smoothing and differentiation have been subjects of intense study. A variety of optimal differential operators have been proposed to solve different computer vision problems (see for example: [8, 13, 14, 37, 53, 63, 68, 69, 78, 79] for edge and line detection and [2, 16, 71] for optical flow estimation). Differentiation is highly sensitive to noise, but can be reduced/avoided using an appropriate scale selection for the smoothing function. However, amplitude-based measurements are sensitive to smooth shading and lighting variations. In particular, this can be a source of serious error, for example for differential optical flow estimation. Moreover, an image contains many types of edges (not only step-edges). For instance, for edge and line detection, one might, for example, combine the outputs of a step detector and line detector. However, this is not a perfect solution since it leads to edge duplication (see for e.g. [66, 79]). Furthermore, especially for medical images such as X-ray mammograms [32], the interesting features in the image often do not have the idealised edge shape; here, we do not only mean blur degradation but also feature combination (for example feature number 4 in Fig. 1 is a combination of a line with a positive step edge). These may considerably reduce the optimality of the filter and lead to unpredictable multiple responses.

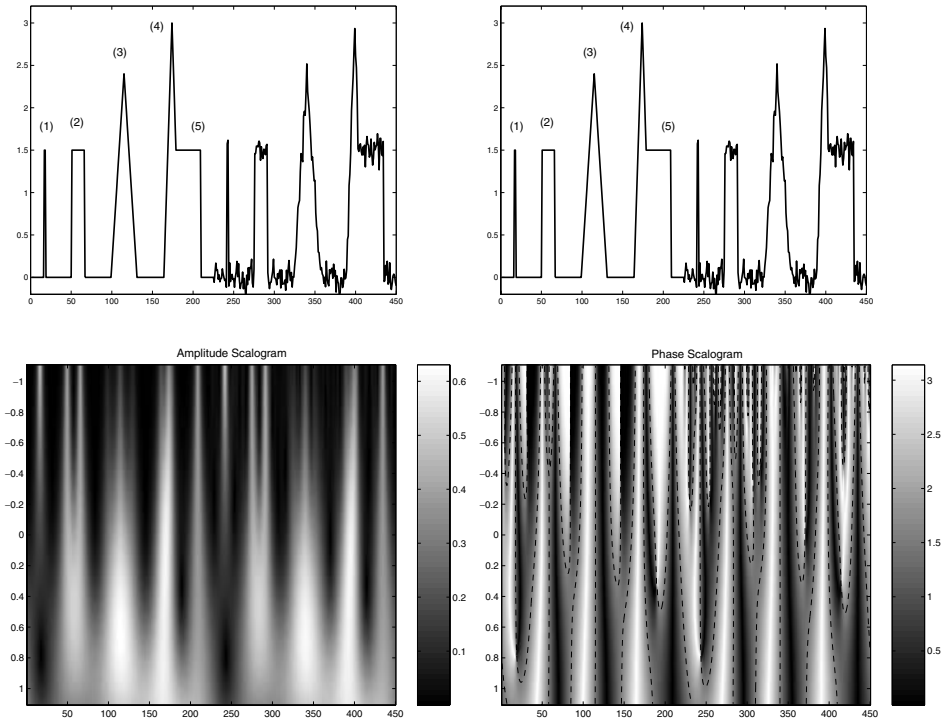

Figure 1. Example of a 1D signal and scalograms of local amplitude (left) and the absolute value of local phase (right). The level contours correspond to a local phase of $\mp\frac{\pi}{2}$ radians. A local phase of $-\frac{\pi}{2}, +\frac{\pi}{2}$, 0 and π corresponds to a valley, a roof(line/bar), a negative step edge and a positive step edge respectively. The scalograms are computed using a difference of Gaussian filter of 2 octaves bandwidth. The vertical axis shows the wavelength of the filter in a log scale $\ln(\frac{\lambda_0}{50})$.

Phase-based feature detection has been investigated extensively following the publication of the Local Energy (LE) model of feature detection [56]. This model postulates that features can be defined and classified using their phase signatures (or their phase congruency (PC)). This observation have led to the development of a number of phase-based feature detection algorithms [18, 31, 39, 58, 61, 64–66, 74]. Phase-based feature detection (PC & LE) provides a *single* unified theory for detecting a wide range of features, rather than being specialised for a single feature type such as intensity steps.

Phase information has also been used successfully for matching and velocity estimation. For instance, phase-difference [36] and phase-correlation [44] techniques have been used for discrete two-view matching and phase gradient used for the measurement of image orientation and optical flow [23, 58].

Numerous additional advantages of the use of phase-based measurements have been reported. Perhaps the most desirable property of phase is that it is theoretically invariant to brightness and contrast. Hence it is, in principle, robust against typical variations in image formation. However, the estimation of phase is intrinsically noisy and depends critically on the choice of the quadrature filters. It is this estimation that we investigate. The key contribution of this paper is to define quantitative performance metrics for quadrature filters to enable a meaningful comparison of filter options to be made and hence to guide the choice of filters in practice.

1.1. Local Phase and Amplitude in 1D Signals

Mathematically, the local properties (Amplitude and Phase) of a 1D real signal (function) $f(x)$ are defined using the so called analytical signal (function) $f_A(x)$ [27]:

$$f_A(x) = f(x) - i f_{\mathcal{H}}(x); \tag{1}$$

where $i = \sqrt{-1}$ and $f_{\mathcal{H}}(x)$ is the Hilbert transform of $f(x)$ defined by:

$$\begin{aligned} f_{\mathcal{H}}(x) &= \frac{1}{\pi} \int_{-\infty}^{\infty} \frac{f(\tau)}{\tau - x}\, d\tau \\ \Leftrightarrow F_{\mathcal{H}}(\omega) &= F(\omega) \cdot i\, \mathrm{sign}(\omega), \end{aligned} \tag{2}$$

where, $F(\omega)$ is the Fourier transform[2] of $f(x)$ and

$$\text{sign}(\omega) = \begin{cases} -1 & \omega < 0 \\ +1 & \omega \geq 0 \end{cases}.$$

It is straightforward from (1) and (2) to see that:

$$F_A(\omega) = F(\omega) \cdot [1 + \text{sign}(\omega)]. \tag{3}$$

Hence, the analytical signal corresponding to f is obtained by suppressing all its negative frequencies and multiplying all its positive frequencies by two. Given the definition of the analytical signal, we can make the following definitions:

the local amplitude[3] of $f(x)$:

$$A(x) = \| f_A(x) \| = \sqrt{f^2(x) + f^2_{\mathcal{H}}(x)}. \tag{4}$$

and the local phase by:

$$\phi(x) = \arg(f_A(x)) = \arctan\{f(x)/f_{\mathcal{H}}(x)\}. \tag{5}$$

From the above definition of local phase we can derive a number of phase signatures for different image features (see for e.g. [27, 74]). However, direct calculation of these local quantities, as defined above, cannot be done in a phase-based technique. This is mainly because the Hilbert transform/analytical signal, as one can see from equation (2) and (3), is defined over the whole signal/spectrum of the signal; while, for example, for feature detection, localisation in both space and frequency are highly desirable. In other words, we have to design an operator to approximate these quantities in a small, spatial span and over a narrow range of frequencies (scales) to enhance spatial localisation and to avoid the effect of noise. One way is to 'window' the function f, $f_w(x) = w(x) \times f(x)$, using, for example, a Gaussian function as $w(x)$ leading to the Short-Time Fourier Transform (STFT) (see for e.g. [51, chap. 4]).

An alternative approach is to estimate the local phase/energy of a filtered version of the signal. One property which this should satisfy is a zero response for a constant signal (to be invariant to grey level shift [65]), which implies that the approximation filter $f_e(x)$ must be:

(1) a band-pass filter (zero DC).
(2) symmetric (with constant phase, so as not to change the phase information of the original signal). The symmetry condition implies that the filter must be even (hence which is why it is denoted f_e).

We then have:

$$\begin{aligned} \hat{f}_A(x) &= f_e(x) \circledast f(x) - i\,\mathcal{H}(f_e(x) \circledast f(x)) \\ &= (f_e(x) - i\,\mathcal{H}(f_e(x)) \circledast f(x) \\ &= (f_e(x) - i\ f_o(x)) \circledast f(x). \end{aligned} \tag{6}$$

where "$\circledast$" denotes the 1-D convolution operator and $f_o(x)$ is the Hilbert transform of $f_e(x)$, hence they are in quadrature. It can be shown, given the definition of the Hilbert transform and the Hermitian property of the Fourier transform, that $f_o(x)$ is an odd, zero-DC band-pass filter (see e.g. [27]).

In practice, the computation of an approximation of the local phase and the local amplitude uses a pair of band-pass quadrature filters (an odd filter $f_o(x)$ and an even filter $f_e(x)$), where:

$$\hat{\phi}(x) = \arctan\{f_e(x) \circledast f(x)/f_o(x) \circledast f(x)\}, \tag{7}$$

$$\hat{A}(x) = \sqrt{[f_e(x) \circledast f(x)]^2 + [f_o(x) \circledast f(x)]^2}. \tag{8}$$

An example of an amplitude scalogram and a phase scalogram of a 1D signal is shown in Fig. 1. The signal is a combination of different type of edges; the first part of the signal is an ideal profile and the last part is a noisy version of the signal (additive white Gaussian noise with a signal-to-noise = 18 dB). Observe that all the features, independently of their shapes, are detected and can be classified using their phases. However the interpretation of a type of feature is obviously scale dependent. Consider for example the second feature: inspecting the amplitude scalogram we notice that at small scales, the feature is detected as a positive step edge followed by a negative step edge; however at very large scales there is only one peak in the amplitude scalogram and the corresponding phase at this maximum is the phase of a line. Notice for example the first feature is no longer detected at large scales; the amplitude scalogram shows a black spot and the corresponding phase is not defined, this point in scale space is called a singularity point.

1.2. Multidimensional Signals

The analytical signal and the corresponding quadrature filters provides a powerful framework for the extraction of local properties of signals. Until recently, two (and more generally N-) dimensional signal theory suffered from the absence of an *isotropic* extension of the analytical signal/Hilbert transform. Several attempts

to generalise the Hilbert transform may be found in the literature [20]: for instance, the directional/partial Hilbert transform [27, 66], the total Hilbert transform [28], and a combination of these two in the Fourier domain [28] and in the quaternionic Fourier domain [6]. Unfortunately, none of these approaches satisfy the isotropy property, which is necessary to obtain invariance with respect to orientation. Hence, other implementations have been proposed in the literature, for two-dimensional signals via the use of steerable filters [25, 72] or by performing the analysis at a set of orientations, then combining the results to provide the information at any orientation in the image [29, 31, 40, 47, 57, 58, 61, 64, 74].

Recently, Felsberg and Sommer [19, 20] proposed a novel two-dimensional generalisation of the analytic signal based on the Riesz transform, which is used instead of the Hilbert transform. A 2D isotropic analytic signal, the *monogenic signal*, is proposed. This representation preserves the core properties of the 1D analytic signal that decomposes a signal into information about structure (local phase) and energy (local amplitude). The basic idea is to design an odd isotropic filter which is vector-valued rather than scalar-valued. The "monogenic signal" is an important "phasor" for describing image properties (local phase, local amplitude and local orientation). The construction of the monogenic signal is straightforward given the 1D quadrature filter; the reader is referred to [20] for more detail.

Several applications of the monogenic signal have been already realised: edge detection and local orientation estimation [18], Moiré interferograms [45] and image denoising in a scale space framework [21].

1.3. Summary

Having introduced the analytical signal, and its extension to the multidimensional case (the monogenic signal), we have a powerful mathematical framework for the estimation of local properties of signals. These properties could be used in a number of different image processing applications. In practice, the estimation framework uses a quadrature pair of band-pass zero-DC linear filters. The construction of the multidimensional pair is straightforward given the 1D pair, or in fact given just one of the filters (the odd or the even). The question which naturally arises is: how should one choose the quadrature pair for a given application. This is the question that is addressed in the remainder of this paper.

2. Common Quadrature Filters

In this section, we study a representative set of the most common quadrature filters in the literature[4] as well as number of new pairs derived from classical feature detectors. We provide the reader with either a mathematical expression of filter properties or a numerical estimation. For simplicity, occasionally, for a given property but different filters, we use the same symbol.

2.1. Gabor Filters

In 1946, Denis Gabor [26] introduced the windowed Fourier transform, also called the Short Time Fourier Transform (STFT). Essentially, instead of using a sinusoidal basis function $e^{i\omega x}$ which is well localised in frequency but not localised in time, he used what are now called "Gabor atoms". These are constructed by translating in time/space and frequency a real and symmetric time/space window g:

$$g_{x_0,\omega_0}(x) = g(x - x_0)\exp[i\omega_0 x]. \tag{9}$$

The energy of g_{x_0,ω_0} is concentrated in the neighbourhood of x_0 over an interval which can be measured by the standard deviation σ_g of $\|g\|^2$. Its Fourier transform is a translation by ω_0 of the Fourier transform G of g. Therefore the energy of g_{x_0,ω_0} is concentrated near ω_0, over an interval of size σ_G. In a time-frequency (scale-space) plane (x, ω), the energy spread of Gabor atoms can be represented as a rectangle of width (σ_g, σ_G) centred on (x_0, ω_0). Such a rectangle is called a "Heisenberg rectangle" [51] and the uncertainty principle shows that its area satisfies:

$$\sigma_g \sigma_G \geq \frac{1}{2}. \tag{10}$$

Equality applies only when g is a Gaussian, in which case the atoms g_{x_0,ω_0} are called Gabor functions.

Gabor functions are used extensively in digital image processing because of their optimality in the sense of the uncertainty principle, and because of their similarity to the responses of simple cells in the primary visual cortex of primates [12, 52, 59, 60]. They have been used, for instance, in texture analysis [1, 4, 15, 35, 41], texture segmentation [34, 35, 43, 75, 76], feature detection [9, 10, 57, 62], motion estimation [23, 36], image representation and coding [46], and segmentation from motion [77].

A one-dimensional Gabor function is a Gaussian modulated complex exponential:

$$g_{b\,(\sigma,\,\omega_0)}(x) = n_c\,\frac{1}{\sqrt{2\pi}\,\sigma}\exp\!\left(-\frac{x^2}{2\,\sigma^2}\right)\exp[i\,\omega_0\,x], \tag{11}$$

$$G_{b\,(\sigma,\,\omega_0)}(\omega) = n_c\exp\!\left(-\frac{\sigma^2}{2}(\omega-\omega_0)^2\right), \tag{12}$$

where $\omega_0 = 2\pi/\lambda_0$ is the peak tuning frequency and n_c is a normalisation constant which is application dependent. Two alternative normalisation conditions have been used most frequently in the literature:[5]

(1) maximum condition:

$$\max_{\omega} G_b(\omega) = 1 \quad \Rightarrow n_c = 1. \tag{13}$$

(2) constant energy condition:

$$\begin{aligned}\|g_b(x)\| &= \int_{-\infty}^{\infty} g_b^{\star}(x)\,g_b(x)\,dx = 1\\ \Rightarrow n_c &= \sqrt{2\sqrt{\pi}\,\sigma}.\end{aligned} \tag{14}$$

The half-response spatial frequency bandwidth β (in octaves) is defined as:

$$\beta = \log_2\left(\frac{\omega_2}{\omega_1}\right), \tag{15}$$

where ω_1 and ω_2 are the solutions of $G_b(\omega)|_{n_c=1} = 1/2$ and $\omega_1 < \omega_2$. It follows that the bandwidth β of the Gabor filter(s) is the following function of $k_\beta = \sigma\,\omega_0$:

$$\beta(k_\beta) = \frac{\ln\left(\frac{k_\beta+\sqrt{2\,\ln(2)}}{k_\beta-\sqrt{2\,\ln(2)}}\right)}{\ln(2)}; \tag{16}$$

alternatively,

$$k_\beta = \sqrt{2\,\ln(2)}\,\frac{2^\beta+1}{2^\beta-1}. \tag{17}$$

A complex scalar $z(\Delta x,\ \Delta\lambda)$ encodes the phase behaviour of the Gabor kernel, in the presence of white Gaussian noise, for a small spatial perturbation $\Delta\,x = x_1 - x_0$, and a small scale perturbation $\Delta\,\lambda = \lambda_1 - \lambda_0$, in the neighbourhood of a scale-space point $\mathbf{p}_0(x_0 = 0, \lambda_0)$:

$$\begin{aligned}z_{g_b}(\Delta x,\ \Delta\lambda) = \sqrt{\frac{2\lambda_1\,\lambda_0}{\lambda_1^2+\lambda_0^2}}\exp\Bigg(&-\frac{k_\beta^2(\lambda_1-\lambda_0)^2}{2\left(\lambda_1^2+\lambda_0^2\right)}\\ &-\frac{2\pi^2\,\Delta x^2}{k_\beta^2\left(\lambda_1^2+\lambda_0^2\right)}+i\,2\pi\,\frac{\lambda_1+\lambda_0}{\lambda_1^2+\lambda_0^2}\,\Delta x\Bigg).\end{aligned} \tag{18}$$

See also Appendix A.

Unfortunately, Gabor functions have several limitations in terms of their direct application in computer vision. First, Gabor filters are non-orthogonal [27] though the family forms a frame (the family is complete but redundant) [46]. Although Gabor functions are well localised, they inevitably have infinite support. Truncation is used in most practical implementations to avoid aliasing. Finally, a Gabor pair is not in quadrature as it has non-zero negative frequencies, and a non-zero DC component (the cosine component does not integrate to zero): The normalised negative energy is:

$$\begin{aligned}\mathrm{NE}_{g_b} &= \frac{\int_{-\infty}^{0} G_b(\omega)^2\,d\omega}{\int_{-\infty}^{\infty} G_b(\omega)^2\,d\omega} = \frac{1}{2}(1-\mathrm{erf}(\sigma\,\omega_0))\\ &= \frac{1}{2}(1-\mathrm{erf}(k_\beta)),\end{aligned} \tag{19}$$

and the DC component is:

$$\begin{aligned}\mathrm{DC}_{g_b} = G_b(0)|_{n_c=1} &= \exp\!\left(-\frac{\sigma^2\,\omega_0^2}{2}\right)\\ &= \exp\!\left(-\frac{k_\beta^2}{2}\right).\end{aligned} \tag{20}$$

Note that both the negative power and the DC component are functions of the bandwidth β. Figure 2 shows the evolution of DC_{g_b} and the root of the negative energy $\sqrt{\mathrm{NE}_{g_b}}$ as functions of the bandwidth. We note that for a small bandwidth ($\beta < 0.7$) DC correction is not needed, as its value is close to the precision of computers (10^{-6}). However, for filters with a broad bandwidth ($\beta > 0.7$), a correction is needed. In the case of feature detection, Heitger et al. [30] and Ronse [65] independently pointed out this problem. Ronse [65] gave a second condition for the filter to be invariant to the addition of a linear ramp. Both authors proposed a DC correction for the even Gabor filter. In recent work, to which the reader is referred to for

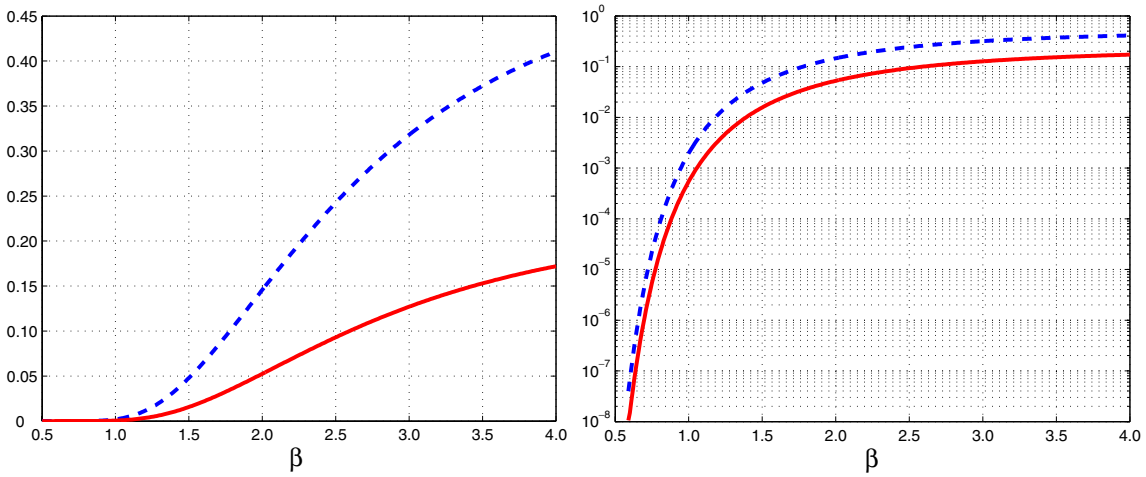

Figure 2. Evolution of DC_{g_b} (dashed curve) and the negative energy $\sqrt{\mathrm{NE}_{g_b}}$ (solid curve) of Gabor filters as a function of bandwidth. Linear scale (left); logarithmic scale (right).

more detail, we studied and compared both corrections; a variant to Ronse's correction is also proposed [3].

2.2. *Log-Gabor Filters*

Log-Gabor (log-Normal) filters have become the preferred choice in many computer vision applications using quadrature filters as they allow arbitrarily large bandwidth zero DC filters to be constructed [18, 19, 22, 27, 40, 58], These filters are particularly suited for the estimation of the local frequency using the ratio of log-Gabor filters [27].

The one-dimensional log-Gabor filter in the frequency domain is a Gaussian function on a logarithmic scale:

$$G_l(\omega) = n_c \exp\left(-\frac{\ln^2(\omega/\omega_0)}{2\,\ln^2(\kappa_\beta)}\right), \tag{21}$$

where ω_0 is the peak tuning frequency and $0 < \kappa_\beta < 1$ is related to the bandwidth β of the filter by the following relation:

$$\beta = -\frac{2\sqrt{2}}{\sqrt{\ln 2}}\,\ln(\kappa_\beta), \tag{22}$$

and inversely:

$$\kappa_\beta = \exp\left(-\frac{1}{4}\sqrt{2\,\ln(2)}\,\beta\right). \tag{23}$$

The two values for the normalisation constant n_c (defined by Eqs. (13) and (14)) are given by:

$$\max_{\omega} G_l(\omega) = 1 \quad \Rightarrow n_c = 1, \tag{24}$$

$$\begin{aligned} &\|g_l(x)\| = \frac{1}{2\,\pi}\|G_l(\omega)\| = 1 \\ &\Rightarrow n_c = \exp\left(-\frac{1}{8}\,\ln(\kappa_\beta)^2\right)\sqrt{-\frac{2\sqrt{\pi}}{\omega_0\,\ln(\kappa_\beta)}}. \end{aligned} \tag{25}$$

The main advantage of log-Gabor filters is that as well as being invariant to a grey-level shift (zero DC) they are also invariant to an additive ramp.[6] A linear operator $f(x)$ is invariant to an additive ramp if and only if:

$$\int_{-\infty}^{\infty} x\, f(x)\, dx = 0. \tag{26}$$

Using the moment property of the Fourier transform, we have:

$$\int_{-\infty}^{\infty} x\, g_l(x)\, dx = i\,\frac{d}{d\,\omega}\, G_l(\omega)|_{\omega=0} = 0. \tag{27}$$

Care must be taken in the design of log-Gabor filters to avoid aliasing. Indeed, the long tails of the filters may run beyond the Nyquist limit imposed by the sampling frequency. Hence, we would like the Nyquist limit to be at least n times the standard deviation away from ω_0 on a logarithmic scale. This gives the following

condition:

$$\omega_0 < \pi\, \kappa_\beta^n. \tag{28}$$

In practice, $n = 3$ is usually sufficient [27].

In addition to the above limit for the central frequency, probably the most significant drawback is the absence of an analytical expression for the filter in the spatial domain.

2.3. *Gaussian Derivative Filters*

Gaussian derivatives are well known in computer vision. This is because of some very desirable properties of the Gaussian function (used as the smoothing function), such as simplicity and steerability. For instance, Gaussian derivatives have been used in feature detection [8, 17, 25, 37, 47, 61, 65, 66] and motion estimation [33, 49].

It is well known that the Fourier transform of a Gaussian function is a Gaussian, and using the derivative property of the Fourier transform, we define the following family of Gaussian derivative quadrature filters in the frequency domain:

$$G_d(\omega) = \begin{cases} n_c\, \omega^a\, \exp[-\sigma^2\omega^2], & \text{if } \omega \geq 0; \\ 0, & \text{otherwise.} \end{cases} \tag{29}$$
$$\text{where,} \quad a \in \mathbb{R} \quad \text{and} \quad a \geq 1.$$

Here, we relax the constraint on a and hence we do not have an analytical expression of the filters in the temporal/spatial domain for $a \notin \mathbb{N}$.

The Hilbert transform of the Gaussian function is the following function (e.g. see [65, 66]):

$$g_{\mathcal{H}}(x) = \frac{\sqrt{2}}{\pi\,\sigma}\,\mathrm{Dw}\left[\frac{x}{\sqrt{2}\,\sigma}\right], \tag{30}$$

where

$$\mathrm{Dw}(x) = \exp(-x^2)\int_0^x \exp(t^2)\,dt \tag{31}$$
$$\text{is the } \textit{Dawson's integral} \text{ function}$$

and

$$\frac{d}{dx}\mathrm{Dw}(x) = 1 - 2\,x\,\mathrm{Dw}(x). \tag{32}$$

The *Dawson's integral* function and its derivatives are shown in Fig. 3. When $a \in \mathbb{N} \subset \mathbb{R}$ and odd, the corresponding odd/even filter in the spatial domain is the ath derivative of the Gaussian/$g_{\mathcal{H}}(x)$, and for even values of a the corresponding odd/even filter is the ath derivative of $g_{\mathcal{H}}(x)$/Gaussian function. This is up to a change of sign and a normalisation factor of $n_c/2$.

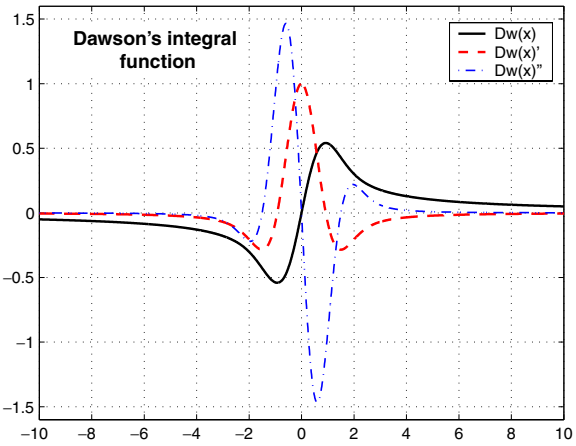

Figure 3. The *Dawson's integral* function and its derivatives in the spatial domain.

It is straightforward to see that the family has zero DC, and that it is therefore invariant to a grey level shift, and for $a > 1$, it is invariant to an additive ramp (see (26)). The two values for the normalisation constant n_c are given by:

$$\max_\omega G_d(\omega) = 1 \quad \Rightarrow n_c = 1/G_d(\omega_0), \tag{33}$$

$$\begin{aligned} \|g_d(x)\| &= \frac{1}{2\,\pi}\|G_d(\omega)\| = 1 \\ \Rightarrow n_c &= 2\,\frac{\sqrt{\pi}\,\sigma^{\left(a+\frac{1}{2}\right)}}{\sqrt{\Gamma\left(a+\frac{1}{2}\right)}}, \end{aligned} \tag{34}$$

where $\Gamma(\cdot)$ is the gamma function and ω_0 is the peak tuning frequency given by:

$$\omega_0 = \frac{\sqrt{a}}{\sigma}. \tag{35}$$

The octave bandwidth of this family is given by:

$$\beta = \frac{\ln\left(\frac{\mathrm{W}(-1,\,c)}{\mathrm{W}(0,\,c)}\right)}{2\,\ln(2)}, \quad \text{with} \quad c = -\frac{4^{-(1/a)}}{e}. \tag{36}$$

Here, $\mathrm{W}(k,\,\cdot)$ is the kth branch of the Lambert's W function [11].

The Gaussian derivative kernels, as defined here, have the advantage of allowing a continuous bandwidth

with a maximum bandwidth of 2.59 octaves corresponding to the 1st derivative. Note that the analytical expression in the spatial domain is only valid for integer derivative values. Differential Gaussian filters exhibit less aliasing than log-Gabor filters.

2.4. Difference of Gaussian Filter (DoG)

The DoG filter has been used in a number of feature detection applications [42, 48, 50, 53, 55] and has been proposed as a filtering model of the human visual system. For example, retinal ganglion cells and lateral geniculate cells early in the visual processing have receptive fields which can be implemented as DoG filters [53, and references therein].

The filter (even) is given by:

$$f_{\mathrm{DoGe}}(x) = \frac{n_c}{\sqrt{2\pi}\,\sigma'} \exp\left(-\frac{x^2}{2\,\sigma'^2}\right) - \frac{n_c}{\sqrt{2\pi}\,\sigma} \exp\left(-\frac{x^2}{2\,\sigma^2}\right), \quad (37)$$

where $\sigma > \sigma' > 0$.

This operator approximates well the second derivative of a Gaussian and has one more degree of freedom.[7] Several authors have specified a preference for it possibly because of its ease of implementation. However, this filter has a far better performance, for line detection, than the 2nd derivative of a Gaussian in the sense of Canny's criteria.

As already noted, the Hilbert transform of the Gaussian function is the Dawson's function given by (30). Hence the odd filter in quadrature with $f_{\mathrm{DoGe}}(x)$ is given by the following:

$$f_{\mathrm{DoGo}}(x) = n_c \frac{\sqrt{2}}{\pi\,\sigma'} \mathrm{Dw}\left[\frac{x}{\sqrt{2}\,\sigma'}\right] - n_c \frac{\sqrt{2}}{\pi\,\sigma} \mathrm{Dw}\left[\frac{x}{\sqrt{2}\,\sigma}\right]. \quad (38)$$

Therefore, the Fourier transform of the quadrature pair is defined by (up to a multiplicative factor of 2):

$$F_{\mathrm{DoG}}(\omega) = \begin{cases} n_c \exp\left(-\frac{\sigma'^2\,\omega^2}{2}\right) - n_c \exp\left(-\frac{\sigma^2\,\omega^2}{2}\right), & \text{if } \omega \geq 0, \\ 0, & \text{otherwise.} \end{cases} \quad (39)$$

and the peak tuning frequency is given by:

$$\omega_0 = \frac{2}{\sigma}\left(\frac{\ln(\gamma)}{(\gamma^2-1)}\right)^{1/2} \quad \text{where, } \gamma = \frac{\sigma'}{\sigma}. \quad (40)$$

The two values for the normalisation constant n_c for this family are given by:

$$\max_{\omega} F_{\mathrm{DoG}}(\omega) = 1 \Rightarrow n_c = 1/F_{\mathrm{DoG}}(\omega_0), \quad (41)$$

$$\|f_{\mathrm{DoG}}(x)\| = \frac{1}{2\,\pi}\|F_{\mathrm{DoG}}(\omega)\| = 1 \Rightarrow n_c = 2\sqrt{\sqrt{\pi}\,\sigma}\left(\frac{1}{\gamma} - \frac{2\sqrt{2}}{\sqrt{1+\gamma^2}} + 1\right)^{-\frac{1}{2}}. \quad (42)$$

The quadrature DoG filter is invariant to grey level shift (zero DC) and invariant to an additive ramp (use Eq. (27) with Eq. (39)).

Unfortunately, we have not been able to derive an analytical expression for the bandwidth of the filter. It's straightforward to note that the bandwidth depends only on the ratio $\gamma = \sigma'/\sigma$. The bandwidth as a function of γ is shown in Fig. 4 (a). Notice that the smallest bandwidth allowable for this family is 1.76 (corresponding to the bandwidth of the 2nd derivative of a Gaussian). The filters for $\lambda_0 = 20$ and for different values of γ are shown in Fig. 4 (b) and (c) on a linear and logarithmic scale respectively. Observe that the tuning frequency must be chosen carefully to avoid aliasing problem especially for small values of γ.

2.5. Cauchy Filter

Cauchy filters have been proposed in [38, 65, 66]. This family does not appear to be well known in the computer vision community. However, this family has some attractive properties as we see below. The Cauchy functions are given by:

$$f_n(x) = \Re\{(1-ix)^{-n-1}\} = \frac{\Re\{(1+ix)^{n+1}\}}{(1+x^2)^{n+1}}; \quad (43)$$

$$g_n(x) = \Im\{(1-ix)^{-n-1}\} = \frac{\Im\{(1+ix)^{n+1}\}}{(1+x^2)^{n+1}}; \quad (44)$$

where $n \in \mathbb{N}$ and determines the number of ripples of the two functions and $\Re(z)/\Im(z)$ is the real/imaginary part of z. f_n and g_n are in quadrature and are integrable

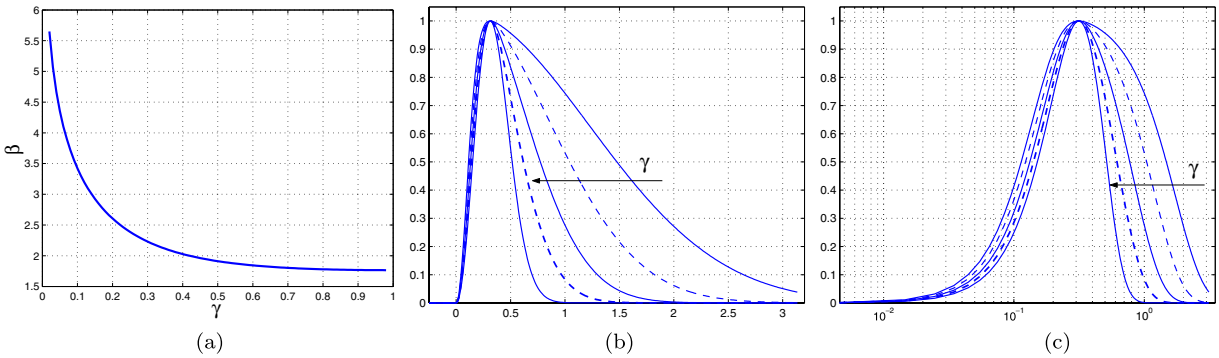

Figure 4. Difference of Gaussian filter. Bandwidth as a function of γ (a); Fourier transform of the filter on a linear (b) and logarithmic (c) scale for $\lambda_0 = 20$ and $(\gamma, \beta) = (0.081, 3.63)$, $(0.131, 3.05)$, $(0.212, 2.53)$, $(0.343, 2.12)$ and $(0.9, 1.76)$. When $\gamma \approx 0.9$ the filter is a good approximation to the 2nd derivative of a Gaussian.

for $n \geq 1$. The Fourier transform of f_n is given by [66]:

$$F_n(\omega) = 2\,\pi\,(n!)^{-1}|\omega|^n \exp(-|\omega|). \tag{45}$$

The values $n = 3$ and $n = 5$ have been proposed to model some properties of the human visual response in [38].

Following the same procedure as for the Gaussian derivatives, we can define a family of quadrature filters using Cauchy functions for $(n = a \geq 1) \in \mathbb{R}$; which in the Fourier domain gives:

$$F_{Ch}(\omega) = \begin{cases} n_c\,\omega^a \exp(-\sigma\,\omega) & \text{if } \omega \geq 0, \\ 0 & \text{otherwise.} \end{cases} \tag{46}$$

where σ is a scaling parameter. Hence, by definition, the filters have zero DC and are invariant to an additive ramp for $a > 1$. Notice that the expression of the filters is similar to that for the Gaussian derivative filters. It can shown that the filters in the spatial domain are given by:

$$\begin{aligned} f_{\text{Che}}(x) &= n_c\,\frac{\Gamma(a+1)}{2\,\pi\,\Re(\sigma - ix)^{a+1}} \\ &= n_c\,\frac{\Gamma(a+1)}{2\,\pi}\,\frac{\Re(\sigma + ix)^{a+1}}{(\sigma^2 + x^2)^{a+1}}, \end{aligned} \tag{47}$$

$$\begin{aligned} f_{\text{Cho}}(x) &= n_c\,\frac{\Gamma(a+1)}{2\,\pi\,\Im(\sigma - ix)^{a+1}} \\ &= n_c\,\frac{\Gamma(a+1)}{2\,\pi}\,\frac{\Im(\sigma + ix)^{a+1}}{(\sigma^2 + x^2)^{a+1}}, \end{aligned} \tag{48}$$

and the normalisation constants are given by:

$$\max_{\omega} F_{Ch}(\omega) = 1 \Rightarrow n_c = 1/F_{Ch}(\omega_0), \tag{49}$$

$$\begin{aligned} \|f_{Ch}(x)\| &= \frac{1}{2\,\pi}\|F_{Ch}(\omega)\| = 1 \\ \Rightarrow n_c &= \left(\frac{\pi\,4^{(a+1)}\,\sigma^{(2\,a+1)}}{\Gamma(2\,a+1)}\right)^{\frac{1}{2}}, \end{aligned} \tag{50}$$

where ω_0 is the peak tuning frequency of the filter and is given by the following ratio:

$$\omega_0 = \frac{a}{\sigma}. \tag{51}$$

The octave bandwidth of this family is given by:

$$\beta = \frac{\ln\left(\frac{\mathrm{W}(-1,c)}{\mathrm{W}(0,c)}\right)}{\ln(2)}, \quad \text{with } c = -\frac{2^{-(1/a)}}{e}. \tag{52}$$

Finally, the complex scalar $z(\Delta x,\ \Delta\lambda)$ which encodes the phase behaviour of this family for a small spatial perturbation $\Delta\,x$, and a small scale perturbation $\Delta\,\lambda$ is given by:

$$\begin{aligned} z_{Ch}(\Delta x, \Delta\lambda) &= \left(\frac{2\sqrt{\sigma_1\,\sigma_0}}{\sigma_1 + \sigma_0 - i\,\Delta x}\right)^{2a+1} \\ &= \left(\frac{2a\sqrt{\lambda_1\,\lambda_0}}{a(\lambda_1 + \lambda_0) - i2\pi\,\Delta x}\right)^{2a+1}. \end{aligned} \tag{53}$$

Figure 5(a) shows the evolution of the bandwidth of the filters function of a. The bandwidth of the Gaussian derivatives is shown for comparison. The transfer function of the quadrature pair is shown on a linear and

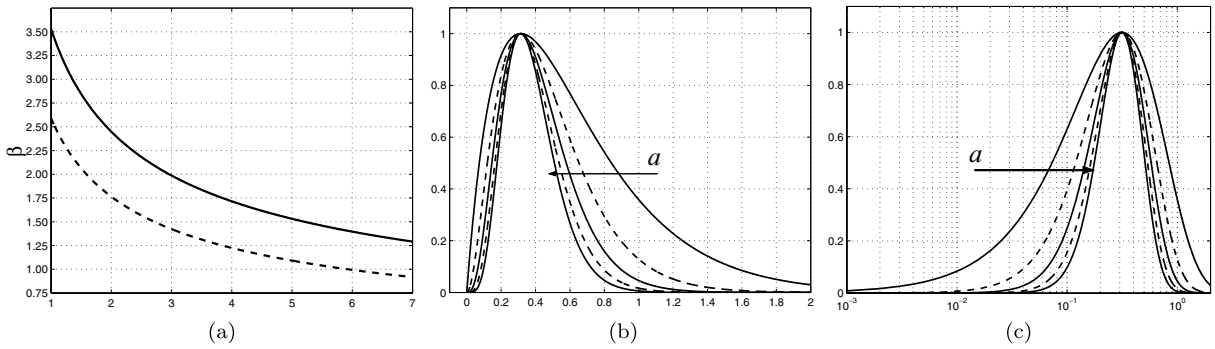

Figure 5. Cauchy quadrature filters; Bandwidth β as a function of a; Cauchy filters (solid curve) and Gaussian derivative filter (dashed curve) (a); Fourier transform of the quadrature pair on a linear (b) and logarithmic (c) scale for $a = 1, 2, 3, 4$ and 5.

logarithmic scale in Fig. 5(b) and (c). Note the similarity of Cauchy functions to the Rayleigh distribution. This may suggest their use as a computationally fast approximation to Rayleigh.

2.6. *Quadrature Filters Related to Canny's Criteria*

Several papers have considered designing optimal edge/line detectors in the sense of Canny's criteria [8] (see Appendix B). These detectors are typically the first/2nd derivative of a smoothing function. To our knowledge, two smoothing functions have been proposed in this sense.

2.6.1. Deriche Filter. We can define a family of quadrature filters using the smoothing function proposed by Deriche [13]. This function is the integral of the optimal operator in the sense of Canny's criteria for edge detection [8]. It is also the smoothing function used by Ziou [80] for optimal line detection according to Canny's criteria. Hence, it is the second integral of the optimal line detector and is given by:

$$s_d(x) = (\alpha|x| + 1)\,\exp(-\alpha|x|), \tag{54}$$

$$S_d(\omega) = \frac{4\alpha^3}{(\omega^2 + \alpha^2)^2}, \tag{55}$$

where α is the scaling parameter ($\sim\sigma^{-1}$).

In a similar way as for Gaussian derivative filters we define a family of quadrature filters in the Fourier domain:

$$F_d(\omega) = \begin{cases} n_c\,\omega^a S_d(\omega), & \text{if } \omega \geq 0; \\ 0, & \text{otherwise.} \end{cases} \quad \text{where, } 1 \leq a \leq 2. \tag{56}$$

The odd filter is the Deriche edge detector for $a = 1$ and the even filter is Ziou's line detector when $a = 2$. The filters are invariant to a grey level shift, and invariant to an additive ramp for $a > 1$ (see Eq. (26)).

It can be shown that the peak tuning frequency is the following function:

$$\omega_0 = \alpha\sqrt{\frac{a}{4-a}}, \tag{57}$$

and, the two values for the normalisation constant n_c are given by:

$$\max_{\omega} F_d(\omega) = 1 \quad \Rightarrow n_c = 1/F_d(\omega_0), \tag{58}$$

$$\|f_d(x)\| = \frac{1}{2\pi}\|F_d(\omega)\| = 1 \quad \Rightarrow n_c = \alpha^{\left(\frac{1}{2}-a\right)}\sqrt{\frac{-12\,\cos(\pi\,a)}{(2\,a-5)(2\,a-3)(2\,a-1)}}. \tag{59}$$

Unfortunately, there is not a simple analytical expression for the bandwidth of the filter. We did a numerical estimation of the bandwidth and approximated its functional dependence on a by the following 4th order

Table 1. Coefficients of the fitting function given by Eq. (60).

i	c_i	μ_i
0	2.54372940760	–
1	0.11940325096	2.00000000000
2	0.01269121401	0.58167860542

polynomial:

$$\beta = c_0 + c_1\left(\frac{a-\mu_1}{\mu_2}\right)^2 + c_2\left(\frac{a-\mu_1}{\mu_2}\right)^4. \quad (60)$$

The coefficients are tabulated in Table 1. The maximum relative error with respect the numerical estimation is 0.0006.

2.6.2. Sarkar and Boyer Filter. Sarkar and Boyer [67] proposed a modification of the multiple response criteria appropriated to the use of IIR filters. Following a similar approach as Canny [8] and Deriche [13], the authors proposed the following smoothing function:

$$s_s(x) = \frac{1}{\alpha}\exp(-\alpha|x|) \times\left\{\cos(\varphi) - \frac{\cos(\alpha\tilde{m}|x|+\varphi) - \tilde{m}\sin(\alpha\tilde{m}|x|+\varphi)}{\tilde{m}^2+1}\right\}, \quad (61)$$

where φ and $\tilde{m}$ determine the shape of the filter and α is the scaling parameter. Note that the above smoothing function is equivalent to Eq. (54) for $\varphi = \frac{\pi}{2}$ and when $\tilde{m} \to 0$.

The Fourier transform of (61) is:

$$S_s(\omega) = 2\alpha^2\tilde{m} \times\frac{(2\sin(\varphi) - \tilde{m}\cos(\varphi))\omega^2 + \alpha^2(\tilde{m}^3\cos(\varphi) + 3\tilde{m}\cos(\varphi) + 2\sin(\varphi))}{(\omega^2+\alpha^2)((\omega+\alpha\tilde{m})^2+\alpha^2)((\omega-\alpha\tilde{m})^2+\alpha^2)}, \quad (62)$$

Hence, we can define the following family of quadrature filters in the Fourier domain:

$$F_s(\omega) = \begin{cases} n_c\omega^a S_s(\omega), & \text{if } \omega \geq 0; \\ 0, & \text{otherwise.} \end{cases} \quad \text{where, } 1 \leq a \leq 2. \quad (63)$$

Unfortunately, the Fourier representation of the filters is not easy to manipulate analytically. Therefore, we studied the filters numerically for $a \in [1, 2]$, and for 4 combinations of the shape parameters $(\tilde{m}, \varphi)$ corresponding to the best values of $\Omega_S(f_s)$, $\Sigma\Gamma(f_s)$, $\Sigma\Gamma = \Omega_S(f_s)$ and $\Sigma\Gamma\Omega_S(f_s)$ for the odd part when $a = 1$ (i.e Sarkar's edge operator). The values are tabulated in Table 2. Figure 6(a) shows the evolution of the bandwidths as a function of a. We first notice a high correlation between the SNR-localisation and the bandwidth

Table 2. Bandwidth and peak tuning frequency of $F_s(\omega)$ for some particular values of the shape parameters.

	$\Sigma\Gamma$	Ω_S	$\tilde{m}$	φ	ω_0/α	β	
	0.885	3.252	1.917	0.651	1.354	2.7007	
$a=1$	2.000	1.622	0.002	1.382	0.5772	3.0096	(*)
	1.833	1.833	0.074	0.120	0.4916	2.9332	
	1.443	2.453	0.464	0.332	0.5355	2.7875	
GD	0.921	3.245	–	–	$\omega_0 = 1/\sigma$	2.5902	
$a=2$	–	–	1.917	0.651	1.7468	1.5554	
	–	–	0.002	1.382	1.0000	2.5431	(*)
	–	–	0.074	0.120	0.8147	2.4012	
	–	–	0.464	0.332	0.8237	2.1393	
GD	–	–	–	–	$\omega_0 = \sqrt{2}/\sigma$	1.7647	

$\Sigma\Gamma$ and Ω_S are given when the odd filter is used for edge detection alone. The Gaussian derivative filter is shown for comparison.

(*) Here the filter is equivalent to the Deriche filter, $\tilde{m} = 0.002$ is the smallest value in our sampling space. Basically the true values for the Deriche filters should be $\tilde{m} = 0$ and $\varphi = \frac{\pi}{2}$.

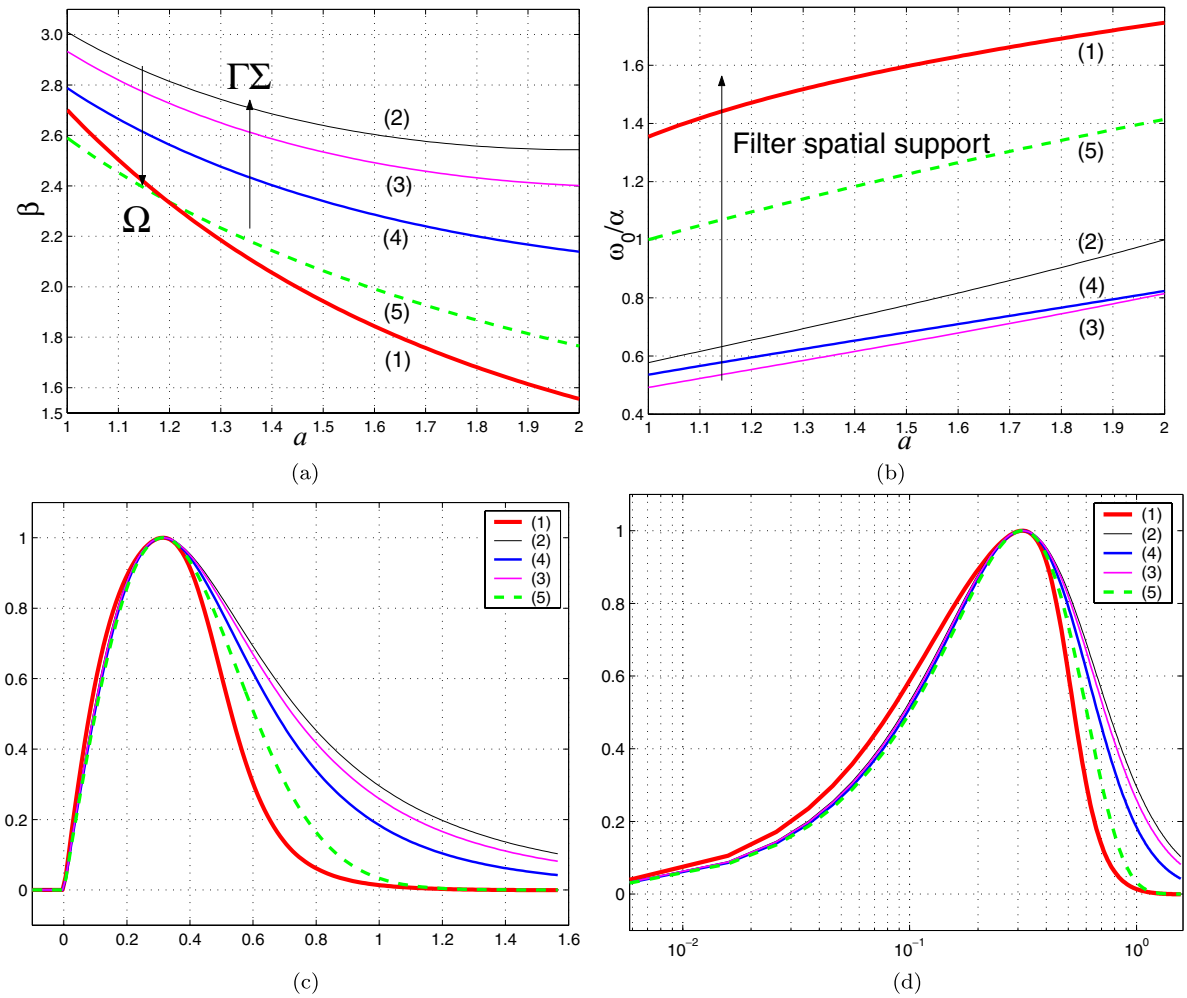

Figure 6. Sarkar and the Deriche filters. Bandwidth as a function of a (a); ω_0/α as a function of a (b); Filters in the Fourier domain on a linear (c) and logarithmic (d) scale for $\lambda_0 = 20$ and $a = 1$. best Ω_S (Red thick curves (1)); best $\Sigma\Gamma$ (Black thin curves (2)); $\Omega_S = \Sigma\Gamma$ (Magenta curves (3)); best $\Sigma\Gamma\Omega_S$ (Blue curves (4)) and Gaussian derivative filter (Green dashed curves (5)). The numbers refer to the same order in Table 2.

of the filters; $\Sigma\Gamma$ increases when β increases. The 1st derivative of the Gaussian is an exception to this rule. We believe that this is mainly due to the difference in the decay of the Gaussian function (exponential) and Sarkar's smoothing function (ω^{a-4}). This is illustrated in Fig. 6(c) and (d). Values of ω_0/α give some insight regarding the spatial support of the filters (see Fig. 6(b)).

We might expect that the performance of a detector depends on its spatial shape. However, this experiment shows the importance of the bandwidth of the filter. Notice that the smallest bandwidth for the edge operators is 2.6 octaves. Several authors mention that larger bandwidths give better results in phase based feature detection [31, 40, 58]. A bandwidth of 1.5 octaves is used in [30, 31, 39, 64], 1.76 octaves in [47, 61] and 2 octaves in [40, 58]; all smaller than 2.6 and even smaller then 2.54 (bandwidth of Ziou's line detector). The second important thing that we can learn from these values, is that even the smallest bandwidth for the edge operators is larger than the largest one for line detectors. Knowing for example that, for the Deriche filter, the odd part alone, for $a = 1$, is optimal in the sense of Canny for edge detection and the even part, for $a = 2$, is optimal in the same sense for lines,[8] this implies that a quadrature pair will not be optimal for both in the sense of Canny. Hence, a tradeoff must be made.

The spatial representation of the filters is shown in Fig. 7. Figure 7(a) and (b) shows the filters for $a = 1$ (i.e odd parts correspond to the edge operators) and Fig. 7(c) and (d) shows the same filters but for a constant bandwidth of 2.5431 octaves (i.e different values of a). Interestingly, the shape (by which we mean the relative differences) of the filters are similar for both cases. Hence we expect the filters to have similar relative performances in the sense of Canny. This experiment shows the importance of filter shape. Notice that a bandwidth of 2.4531 corresponds to $a = 2$ for the Deriche filter (optimal even part) and to $a = 1.032642$ for the Gaussian derivatives (good approximation to the 1st derivative). Inspecting Fig. 7(d), it is more likely that the odd part of a Deriche filter for $a = 2$ will have a better $\Sigma\Gamma$ than the 1st derivative of a Gaussian.

The above experiments highlight issues in choosing a quadrature pair for feature detection and on which basis. It also suggests the possibility of adapting Canny's criteria to the local energy model for the purpose of filter design aiming to have similar performances at least for edges and lines. This is a very delicate point since, for example, the localisation criteria and the multiple responses criteria might not be suitable as they do not take into account the phase information. However, the adaptation of the SNR criteria is straightforward.

We do not have a clear answer to the above questions but they are worthy of further investigation. It is more likely and justified, however, to use a quadrature pair

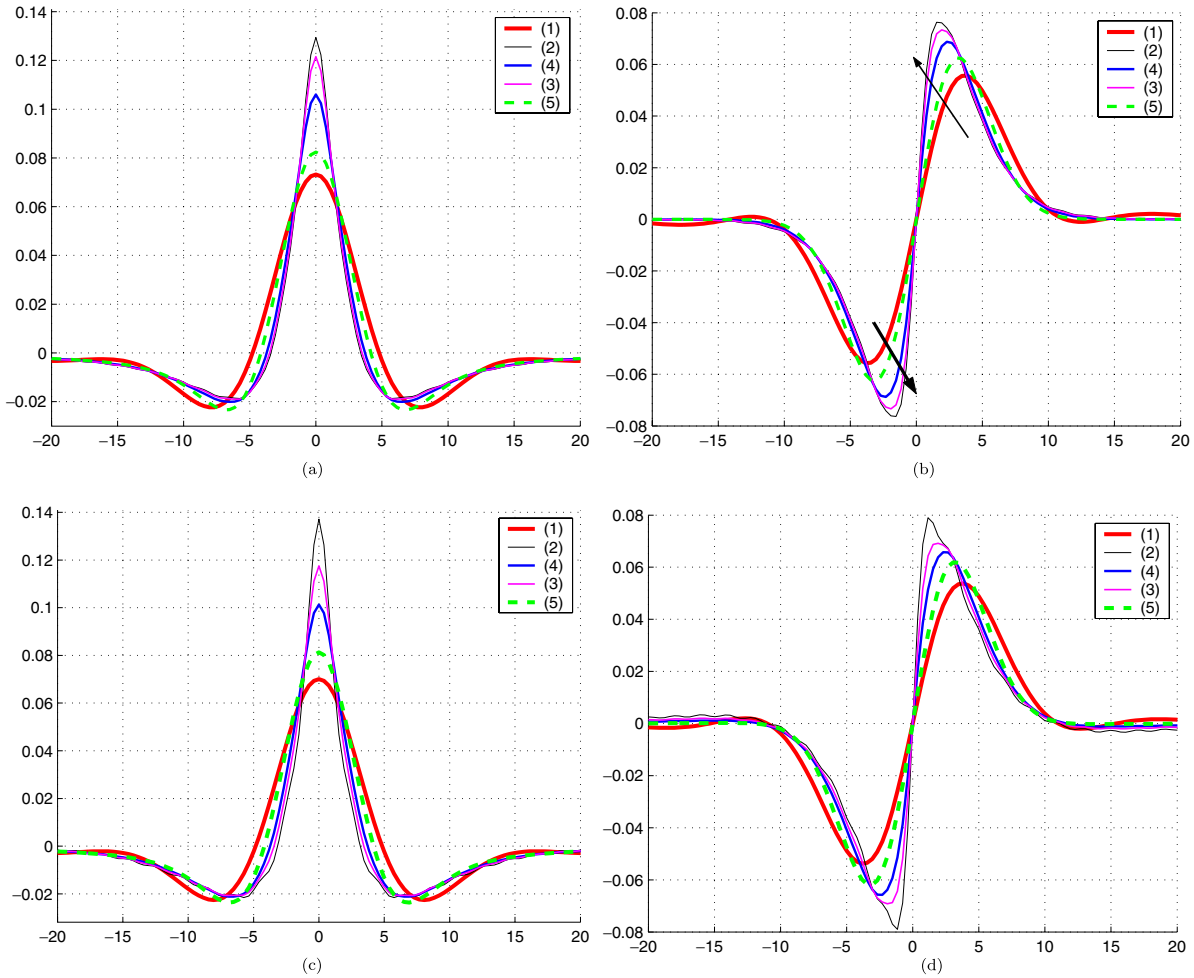

Figure 7. Sarkar and the Deriche filters in the spatial domain for $\lambda_0 = 20$. Constant value of $a = 1$ (a) and (b), the arrows show increasing $\Sigma\Gamma$ (see Fig. 6 (c)–(d) for the Fourier representation); Constant bandwidth $\beta = 2.5431$ octaves (c) and (d). Best Ω_S (Red thick curves); best $\Sigma\Gamma$ (Black thin curves); $\Omega_S = \Sigma\Gamma$ (Megenta curves); best $\Sigma\Gamma\Omega_S$ (Blue curves) and Gaussian derivative filter (Green dashed curves).

where the odd/even part is optimal in the sense of Canny if we are more interested in detecting edges/lines, assuming that the contribution of the even/odd part of the filter is negligible.

3. Comparison

We have presented most of the mathematical properties of the different families in the previous section. A summary of the key equations and properties is given in Table 3. In this section, we present a comparison of the filters used as a quadrature pair. For this purpose, the comparison will be fair only if the filters have the same bandwidth and the same tuning frequency.

Figure 8 shows the five different families of filters (Deriche, DoG, Gaussian Derivative, Cauchy and log-Gabor) for a bandwidth of 2.5431 octaves (Bandwidth of Ziou's line detector) and a wavelength of 20, both in the frequency domain and in the spatial domain. Inspecting the Fourier representation of the filters, we notice that the Gaussian derivative filters have the least aliasing, and the Deriche filter is the worst. Notice also that the three families, Deriche, log-Gabor and the DoG filter are very similar for this bandwidth, and the Cauchy family is between these three filters and the Gaussian derivative filter. This gives us some insight into the behaviour of the filters for feature detection as we know that the even part of the Deriche filter is optimal in the sense of Canny, and the odd part of the Gaussian has a high Ω_S and a low $\Sigma\Gamma$. The log-Gabor filter is an acceptable approximation of Ziou's line detector (even part of the Deriche filter), and has low aliasing. Hence, if we use a Fourier domain implementation, this suggests that the log-Gabor filter is preferable for line detection using this bandwidth.

Figure 9 shows the same five families for the same wavelength of 20 but for a larger bandwidth ($\beta = 3.0096$ octaves) in the frequency domain and in the spatial domain, except for the Gaussian derivative filter where $\beta = 2.5902$ (maximum bandwidth corresponding to the 1st derivative). A bandwidth of 3.0096 octaves corresponds to the Deriche edge operator for the Deriche family which has the best SNR-localisation. First of all, notice that for this bandwidth, the Deriche filter has less aliasing than the log-Gabor filter. This is the opposite relation to before (i.e, when $\beta = 2.5431$ octaves). We remark that the Cauchy filter approximates the Deriche filter quite well and has the advantage of being invariant to an additive ramp besides the fact that Cauchy filters has less aliasing than the Deriche filter. The DoG filter seems to be very similar to the log-Gabor filter except that the DoG filter has less aliasing. Notice that, the DoG filter with this bandwidth (i.e $\gamma = 0.1350$) has a better SNR-localisation than Ziou's optimal line detector (even part of the Deriche filter for $a = 2$) and similar performance in term of the product of the three criteria.

3.1. Phase Stability

Phase stability is very important in phase-based estimation techniques. Stability over scales is important

Table 3. Summary of main equations and filters properties.

	Temporal/Spatial domain	Fourier domain	Bandwidth	Tuning frequency	Zero-DC/ramp invariance
Gabor	$n_c \frac{e^{-\frac{x^2}{2\sigma^2}}}{\sqrt{2\pi}\,\sigma} e^{i\,\omega_0\,x}$	$n_c\, e^{-\frac{\sigma^2}{2}(\omega-\omega_0)^2}$	$\frac{\ln\left(\frac{\sigma\,\omega_0+\sqrt{2\,\ln(2)}}{\sigma\,\omega_0-\sqrt{2\,\ln(2)}}\right)}{\ln(2)}$	ω_0	No/No
log-Gabor	No	$n_c\,\exp\left(-\frac{\ln^2(\omega/\omega_0)}{2\,\ln^2(\kappa_\beta)}\right)$	$-\frac{2\sqrt{2}}{\sqrt{\ln 2}}\,\ln(\kappa_\beta)$	ω_0	Yes/Yes
Gaussian derivative	Only for $a \in \mathbb{N}$	$n_c\,\omega^a\,\exp[-\sigma^2\omega^2]$	$\frac{\ln\left(\frac{W(-1,\,c)}{W(0,\,c)}\right)}{2\,\ln(2)}, c = -\frac{4^{-(1/a)}}{e}$	$\frac{\sqrt{a}}{\sigma}$	Yes/Yes ($a > 1$)
DoG	Yes	$n_c\left(e^{-\frac{\sigma'^2\omega^2}{2}} - e^{-\frac{\sigma^2\omega^2}{2}}\right)$	Numerical (Fig. 4 (a))	$\frac{2}{\sigma}\sqrt{\frac{\ln(\gamma)}{(\gamma^2-1)}}, \gamma = \frac{\sigma'}{\sigma}$	Yes/Yes
Cauchy	$n_c\,\frac{\Gamma(a+1)}{2\pi\,(\sigma-ix)^{a+1}}$	$n_c\,\omega^a\,\exp(-\sigma\,\omega)$	$\frac{\ln\left(\frac{W(-1,\,c)}{W(0,\,c)}\right)}{\ln(2)} c = -\frac{2^{-(1/a)}}{e}$	$\frac{a}{\sigma}$	Yes/Yes ($a > 1$)
Deriche	No	$n_c\,\omega^a\,\frac{4\,\alpha^3}{(\omega^2+\alpha^2)^2}$	Numerical Fig. 6(a)	$\alpha\sqrt{\frac{a}{4-a}}$	Yes/Yes ($a > 1$)
Sarkar and Boyer	No	Yes (*)	Numerical Fig. 6 (a)	Numerical Fig. 6 (b)	Yes/Yes ($a > 1$)

(*) $2\,n_c\,\omega^a\alpha^2\,\tilde{m}\,\frac{(2\,\sin(\varphi)-\tilde{m}\,\cos(\varphi))\,\omega^2+\alpha^2\,(\tilde{m}^3\,\cos(\varphi)+3\,\tilde{m}\,\cos(\varphi)+2\,\sin(\varphi))}{(\omega^2+\alpha^2)((\omega+\alpha\,\tilde{m})^2+\alpha^2)((\omega-\alpha\,\tilde{m})^2+\alpha^2)}$.

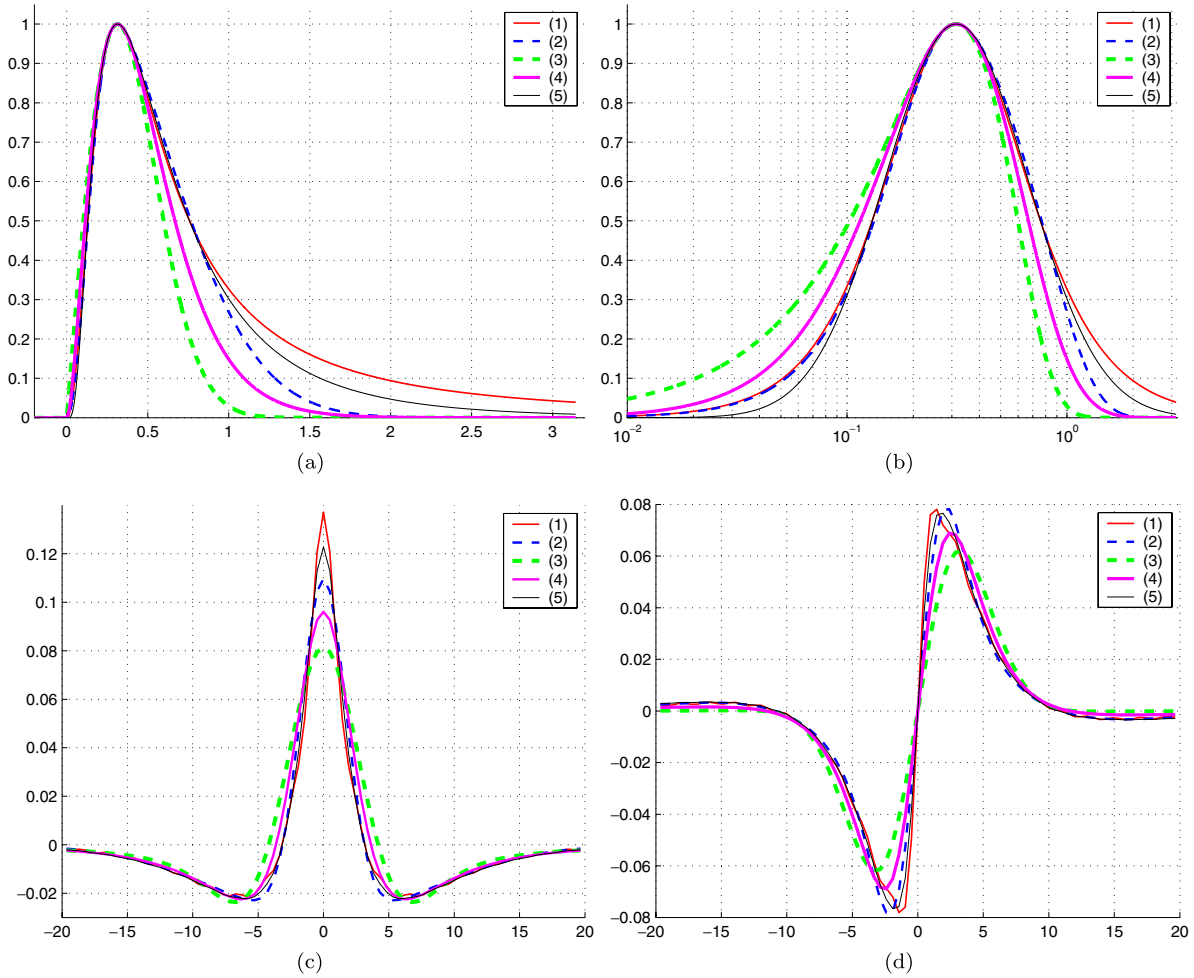

Figure 8. Different quadrature filters in the frequency domain (a) and (b) and in the spatial domain, even part (c) and odd part (d). All the filters have a bandwidth of $\beta = 2.5431$ octaves and a peak tuning frequency for $\lambda_0 = 20$. Deriche filter with $a = 2$ (Red solid curves (1)); DoG filter with $\gamma = 0.215$ (Blue dashed curves (2)); Gaussian derivative with $a = 1.0326$ (Green dashed curves (3)); Cauchy filters with $a = 1.8597$ (Megenta solid curves (4)) and log-Gabor filters with $\kappa_\beta = 0.4730$ (Black solid curves (5)).

for example in feature detection using Phase Congruency and the linearity of phase with respect to a space perturbation is more important in velocity estimation. It is also desirable to know the error in measurement of phase due to the presence of noise. This could for example be taken into account in a regularisation framework of the estimation/detection.

Fleet and Jepson [24] studied the phase behaviour of quadrature filters with respect to a scale-space perturbation $(\Delta x, \Delta\lambda)$ in the neighbourhood of a scale-space point $\mathbf{p}_0(0, \lambda_0)$ in the presence of white Gaussian noise. A short summary of their main results is given in Appendix A. The authors derived an approximation to the expected mean $\mu(z)$ of phase difference $\Delta\phi$, and an upper bound of the expected mean variation $b(z)$ about the mean phase difference $\mu(z)$. $\mu(z)$ is independent of the bandwidth of the filters but $b(z)$ is not. Phase is perfectly stable when $\Delta\phi$ is constant with respect to changes in scale $\Delta\lambda$; and it is linear with respect to spatial position when $\Delta\phi$ is a linear function of Δx (i.e stability through scale and linearity through space near $\mathbf{p}_0$). Earlier, in this paper, we provided analytical expressions for phase behaviour for the Gabor and Cauchy kernels, and we studied the others numerically.

Figure 10 shows the level contours of the mean phase difference $\mu(z)$, for five families: Deriche, DoG,

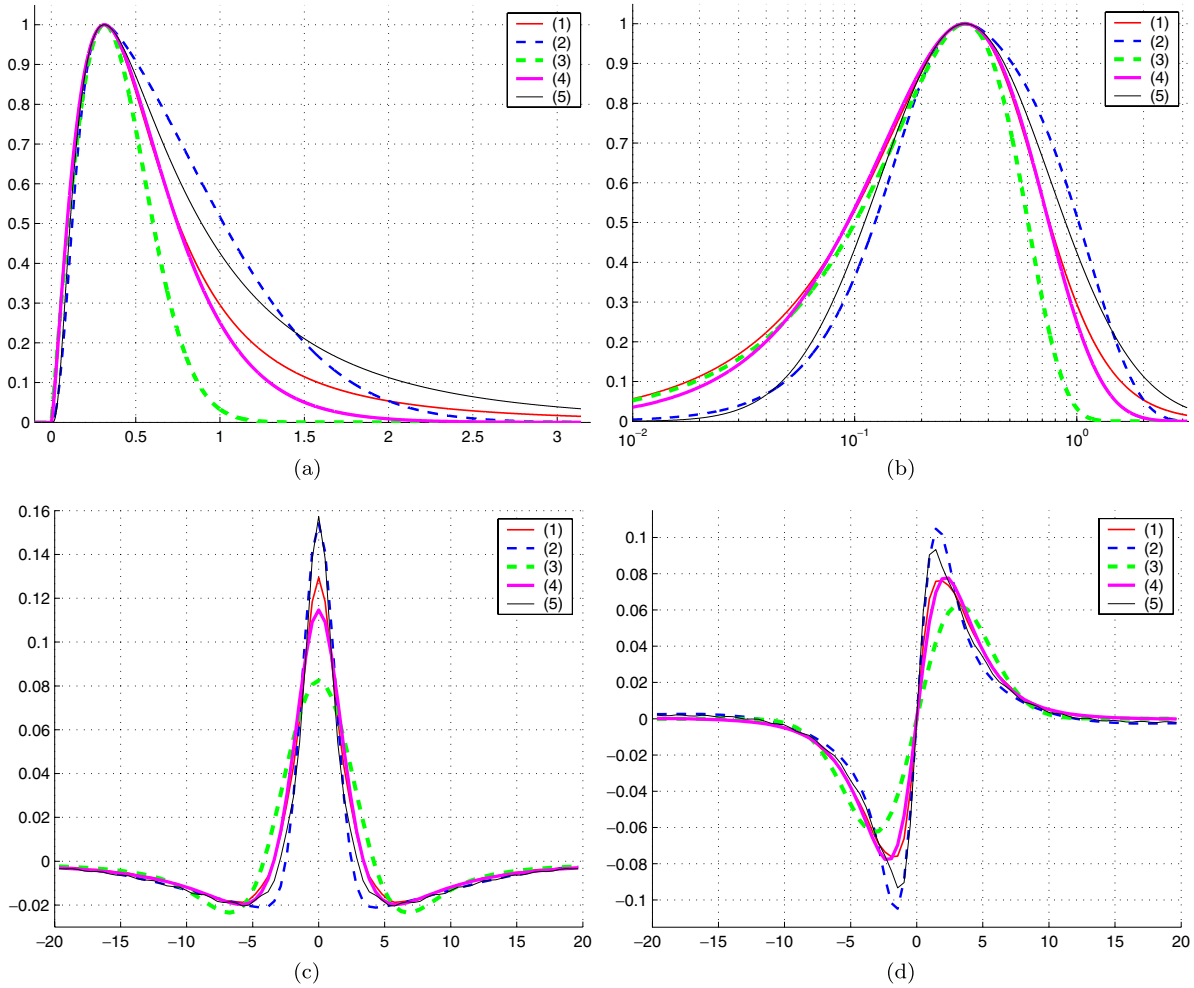

Figure 9. Quadrature filters in the frequency domain (a) and (b) in the spatial domain, even part (c) and odd part (d). All the filters have a bandwidth of $\beta = 3.0096$ octaves (except Gaussian derivative $\beta = 2.5902$) and a peak tuning frequency for $\lambda_0 = 20$. Deriche filter with $a = 1$ (Red solid curves curves (1)); DoG filter with $\gamma = 0.1350$ (Blue dashed curves (2)); Gaussian derivative with $a = 1$ (Green dashed curves (3)); Cauchy filters with $a = 1.3486$ (Megenta solid curves (4)) and log-Gabor filters with $\kappa_\beta = 0.4124$ (Black solid curves (5)).

Cauchy and log-Gabor for $\beta = 3.0096$ and the 1st derivative of a Gaussian for $\beta = 2.5902$. In theory $\mu(z)$ is independent of the bandwidth of the filters, if the self-similarity condition A.7 is satisfied. This figure illustrates that phase is stable over scale for all the families. However the linearity through space is not perfect for some of them for this bandwidth. This is illustrated in Fig. 10 (Profiles), showing $\mu(z)$ as a function of Δx when $\lambda_1 = \lambda_0$.

We find that phase is perfectly linear only for the 1st derivative of a Gaussian when $-\frac{\lambda_0}{2} \leq x_1 \leq \frac{\lambda_0}{2}$; Cauchy filters and the Deriche filter have a similar behaviour and are close to linear in this range. However the phase is still linear in the vicinity of $\mathbf{p}_0$ for all filters. The DoG and log-Gabor kernels have the largest phase distortion. This is a consequence of the tailed nature of the two families for large bandwidths. Inspecting the errors on the mean estimation shown in Fig. 11, we notice that it is for these two families that we have the largest error bound for a spatial perturbation and the smallest for a scale perturbation. This observation, as well, is a consequence of the tailed nature of the log-Gabor and the DoG kernels. As mentioned by Fleet and Jepson [24], as the bandwidth increases, the spatial span of the kernels decreases, and therefore there is a decrease in the spatial extent over which phase is linear. On the other hand, an increase in bandwidth implies that filters tuned to nearby scales will overlap to a great

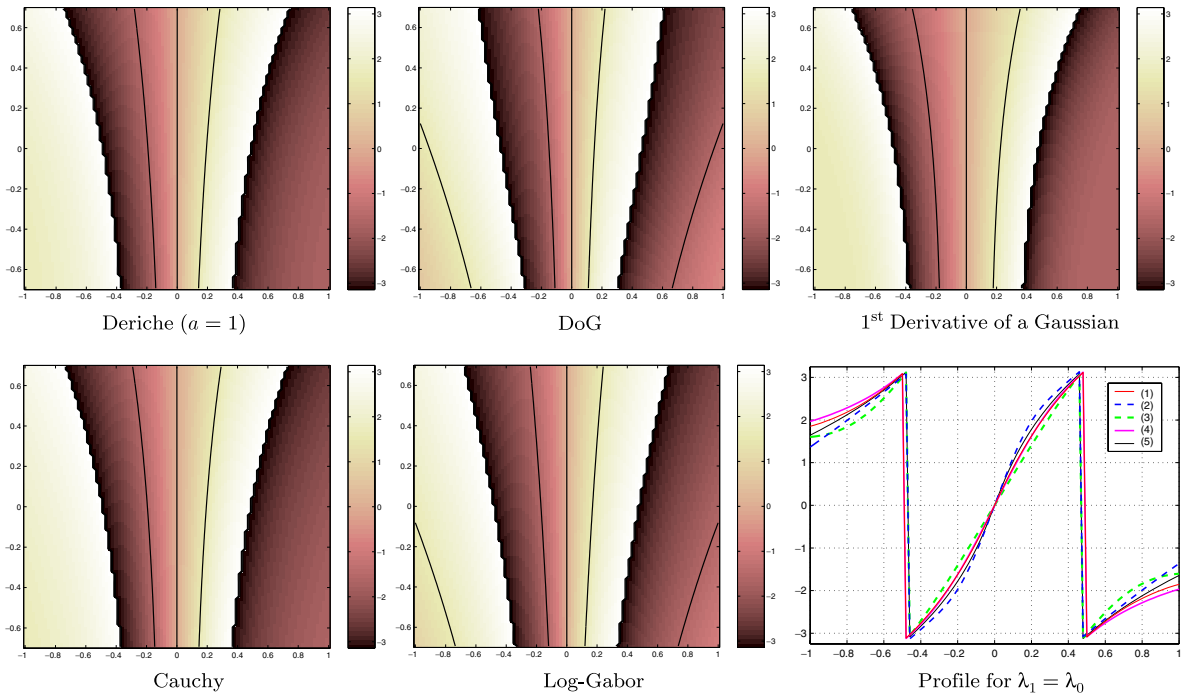

Figure 10. Mean phase difference level contours $\mu(z) = n\,\pi/2$, with $n = -4, \ldots, 4$, near $\mathbf{p}_0 = (0, \lambda_0)$ with a log scale on the vertical axis over two octaves $\frac{\lambda_1}{\lambda_0} \in [\frac{1}{2}, 2]$, and spatial position on the horizontal axis, $\frac{x_1}{\lambda_0} \in [-1, 1]$. All the filters have a bandwidth of 3.0096 octaves except for the 1st derivative of a Gaussian.

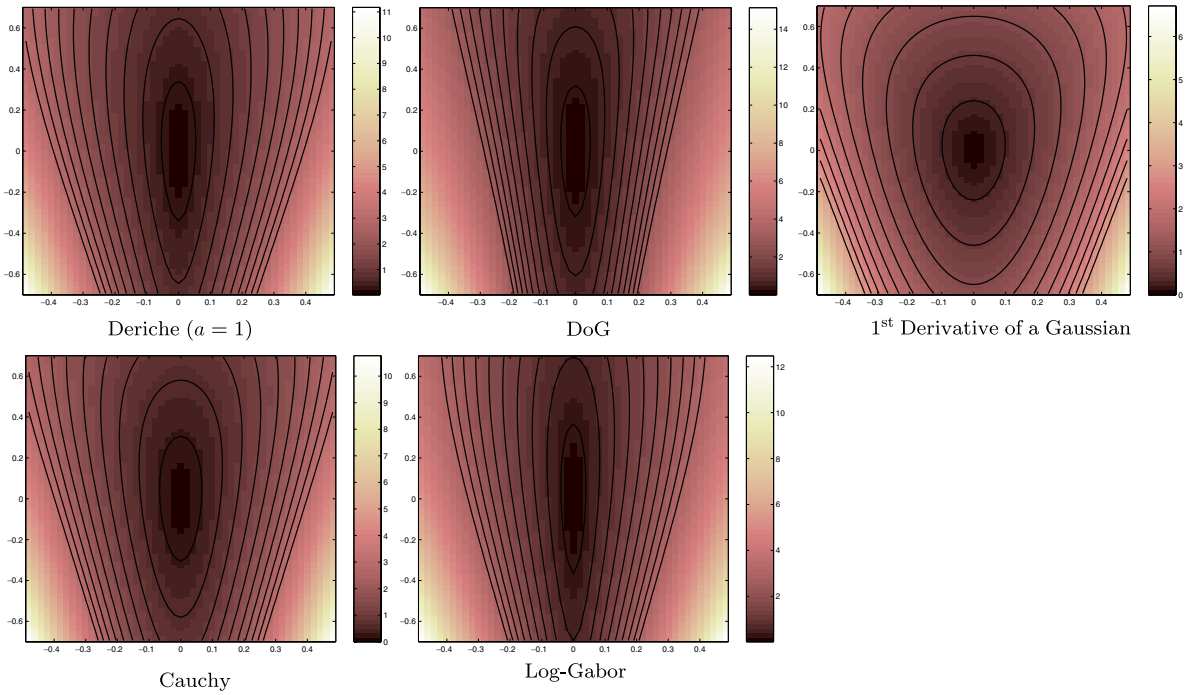

Figure 11. Level contours $b(z) = 0.3\,n$, with $n = 1, \ldots, 10$, corresponding to $\mu(z)$ shown in Fig. 10. All the filters have a bandwidth of 3.0096 octaves except for the 1st derivative of a Gaussian.

extent, and therefore phase is stable for larger scale perturbations. The 1st derivative of a Gaussian has a smaller bandwidth in this experiment, hence, phase is linear for a larger extent. Regarding the other kernels, the larger the extent of the kernel in the Fourier domain, the less is the extent of phase linearity.

Notice that there is a trade-off for the bandwidth between the scale perturbation on the mean phase error $b(z)$, and the spatial one. We will come back to this point when analysing stability for small bandwidths below.

Figure 12, shows the same measures $\mu(z)$ and $b(z)$ for a smaller bandwidth $\beta = 2.5431$ octaves (corresponds to the bandwidth of Ziou's line detector). We notice the same observations regarding the error on the expected mean phase as before. Notice that as the bandwidth of the filters decreases, the expected deviation form $\mu(z)$ is reduced for spatial perturbations and increases for scale perturbations. This is not the case for the Deriche filter, for which the effect is slightly the opposite (see for example the difference between the DoG filter and the Deriche filter). Indeed, as we already mentioned in the last section (see Fig. 8), the Deriche filter has the largest aliasing for this bandwidth (larger than for $\beta = 3.0069$, i.e $a = 1$). This is due to the decay of the Fourier transform of this family ($\omega^{(a-4)}$). Regarding the phase linearity of the filters, as expected, we notice that the extent over which phase is linear has increased.

The phase behaviour for a bandwidth of $\beta = 1.8$ octaves is shown in Fig. 13 for: Gabor kernels with zero DC correction [3], DoG, derivative of a Gaussian, Cauchy and log-Gabor kernels. We did not show the Deriche filters result as the smallest bandwidth of this family is 2.54 octaves. For $\beta = 1.8$, all the filters are perfectly linear for spatial perturbations of more than half of a wavelength. Notice the similar behaviour in terms of the expected deviation $b(z)$ for Gabor, DoG and the Gaussian derivative filters. Notice that a Gaussian derivative filter of a bandwidth of 1.8 octaves corresponds to $a = 1.92$ and a DoG filter of the same bandwidth has a value of 0.7 for γ. Hence, the similarity between the DoG filter and the derivative of a Gaussian filter is expected for this bandwidth, as we know that the 2nd derivative of a Gaussian is well approximated by the DoG filter for $\gamma \approx 0.9$ and that the shape variability of the DoG filter is very low when $\gamma > 0.5$ (see Fig. 4).

Finally, Fig. 14 shows $\mu(z)$ and $b(z)$ for a bandwidth of $\beta = 1$ octave for: Gabor kernels with ([3] and [65]) as zero DC correction, DoG, derivative of a Gaussian, Cauchy and log-Gabor filters. All the families have a linear phase over the range of x_1. All the filters have a comparable errors on the estimation of the mean phase. Notice, the circular shape of the level contours of $b(z)$. As we mentioned before, for small bandwidths, the expected deviation from the mean phase for spatial perturbations of the input is reduced and there is an increase of the spatial extent over which phase is linear. On the other hand, there is an increase of the error bound for scale perturbations which decreases the extent of phase stability.

3.2. Uncertainty Principle

The uncertainty principle criteria is a measure of the scale-space localisation of the filters. Gabor functions are known to be optimal in this sense [see e.g. 51, Chap. 2]. Figure 15 shows the standard deviations of the energy of the filters in the spatial domain σ_f and in the frequency domain σ_F and the uncertainty principle, which is the product of both, $\sigma_f \sigma_F$; all as a function of the bandwidth of the filters and for a peak tuning frequency for $\lambda_0 = 20$. σ_f and σ_F are dependent on λ_0 but not the product. The families used in this experiment are: Cauchy filters (1), Gabor with Ronse zero DC correction using $\tilde{\sigma} = \sigma$ (2) and $\tilde{\sigma} = \breve{\sigma}$ (3), DoG filters (4), Gaussian derivative filters (5), log-Gabor (6) and Sarkar and Boyer filters for best $\Gamma\Sigma$ (i.e Deriche filter) (7) and best $\Gamma\Sigma\Omega_S$ (8).

Inspecting Fig. 15(a), which shows the spatial standard deviations of the filter's energy as a function of the bandwidth, we notice that all the families have a similar spatial extent for small bandwidths ($\beta < 1.5$). For larger bandwidths, the Gaussian derivative and the corrected Gabor wavelets have the largest σ_f. The three following families: Cauchy, log-Gabor and the DoG filters have a very similar σ_f (the DoG filter being the well localised when $\beta > 2.1$ and the worst for $1.76 < \beta < 1.9$). Interestingly, the dependence of σ_f on the bandwidth for the Deriche filter and the Sarkar and Boyer filter is very low.

In the Fourier domain, the corrected Gabor filters have the best localisation followed by the Gaussian derivative family (see Fig. 15(b)). The behaviour of the Cauchy filters is between the Gaussian derivatives and the log-Gabor, which has the worst frequency localisation. The DoG filter has a better localisation than Cauchy kernels for $1.76 < \beta < 2$ and is worse when $\beta > 2$. Here too, we notice that the dependence of σ_F on the bandwidth for Deriche filters and

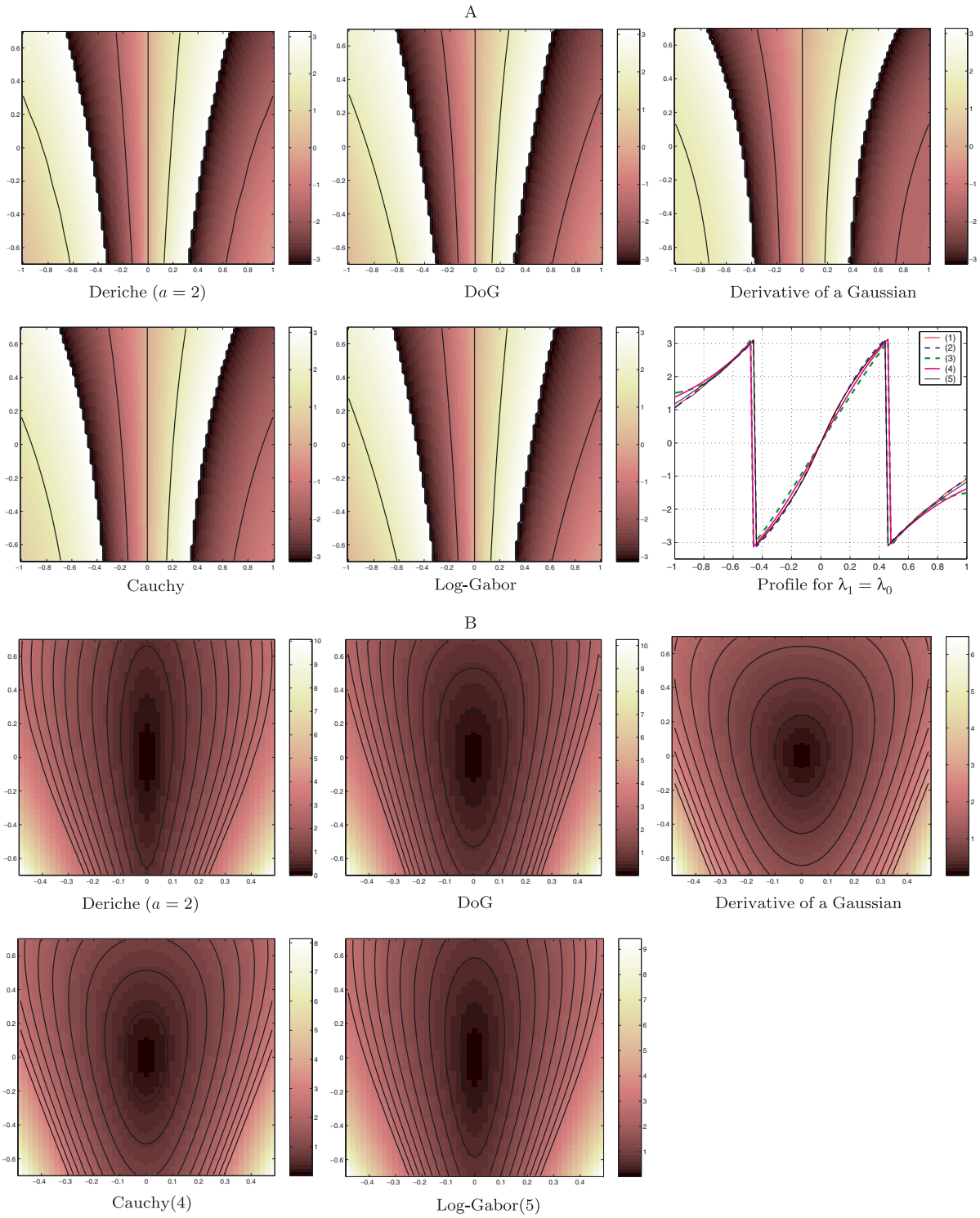

Figure 12. Mean phase difference level contours $\mu(z) = n\,\pi/2$, with $n = -4, \ldots, 4$ (A) and level contours of $b(z) = 0.3\,n$, with $n = 1, \ldots, 10$ (B), near $\mathbf{p}_0 = (0, \lambda_0)$ with a log scale on the vertical axis over two octaves $\frac{\lambda_1}{\lambda_0} \in [\frac{1}{2}, 2]$, and spatial position on the horizontal axis, $\frac{x_1}{\lambda_0} \in [-1, 1]$. All the filters have a bandwidth of 2.5431 octaves.

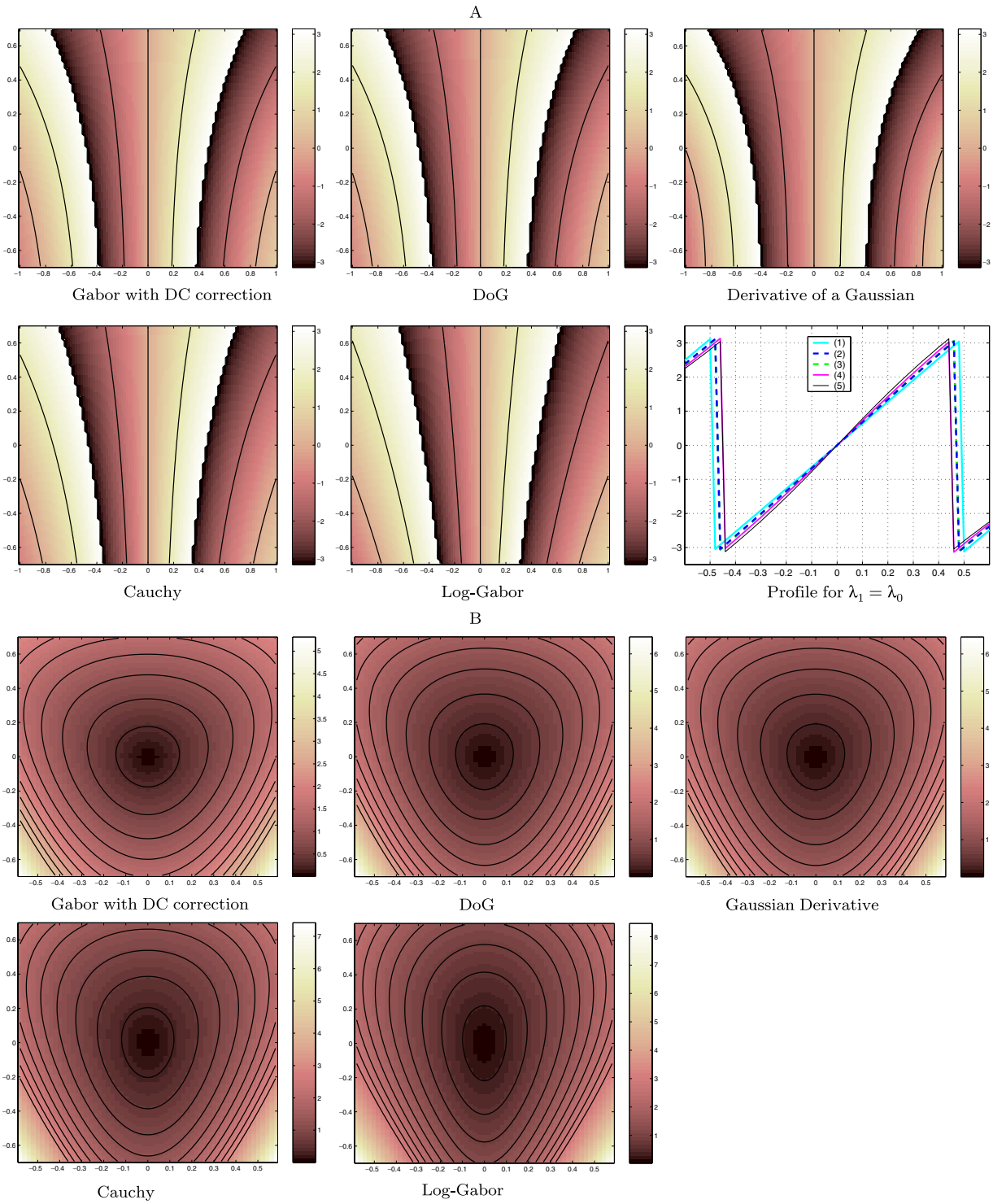

Figure 13. Mean phase difference level contours $\mu(z) = n\,\pi/2$, with $n = -4, \ldots, 4$ (A), and Level contours $b(z) = 0.3\,n$, with $n = 1, \ldots, 10$ (B), near $\mathbf{p}_0 = (0, \lambda_0)$ with a log scale on the vertical axis over two octaves $\frac{\lambda_1}{\lambda_0} \in [\frac{1}{2}, 2]$, and spatial position on the horizontal axis, $\frac{x_1}{\lambda_0} \in [-1, 1]$. The Gabor zero DC correction is obtained with [3]. All the filters have a bandwidth of $\beta = 1.8$.

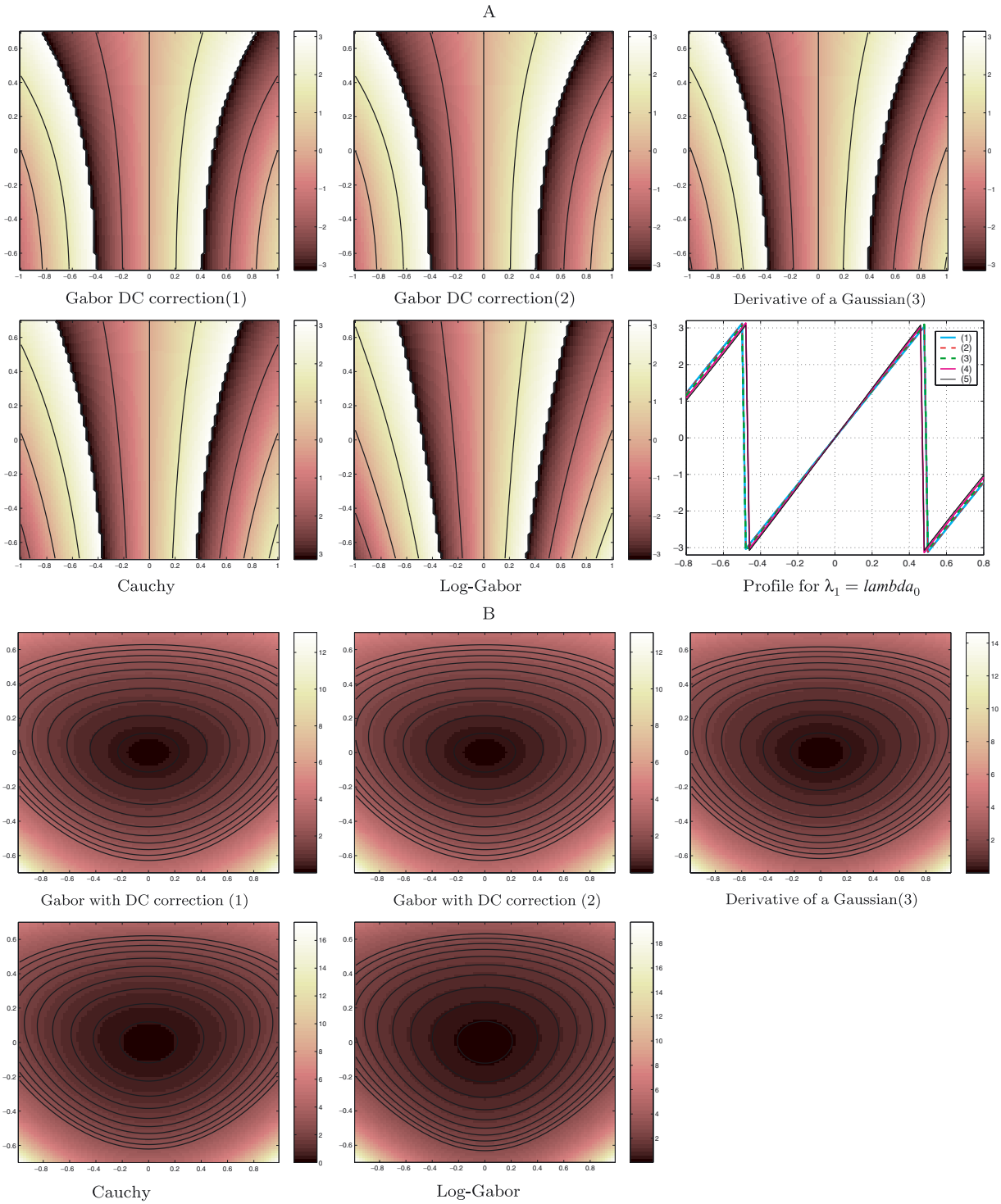

Figure 14. Mean phase difference level contours $\mu(z) = n\,\pi/2$, with $n = -4, \ldots, 4$ (A), and Level contours $b(z) = 0.3\,n$, with $n = 1, \ldots, 10$ (B), near $\mathbf{p}_0 = (0, \lambda_0)$ with a log scale on the vertical axis over two octaves $\frac{\lambda_1}{\lambda_0} \in [\frac{1}{2}, 2]$, and spatial position on the horizontal axis, $\frac{x_1}{\lambda_0} \in [-1, 1]$. Gabor (with [3] as zero DC correction) (1); Gabor (with [65] as zero DC correction) (2). All the filters have a bandwidth of $\beta = 1$.

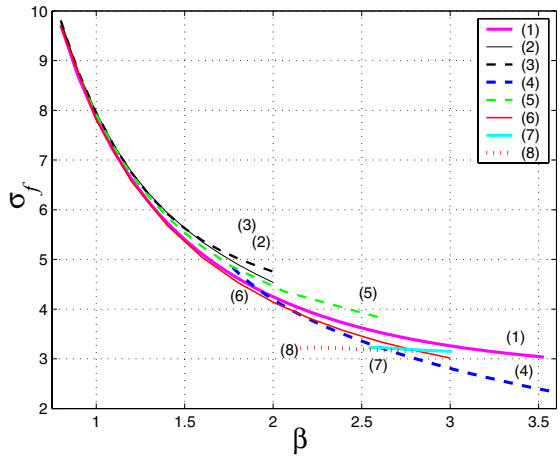

(a)

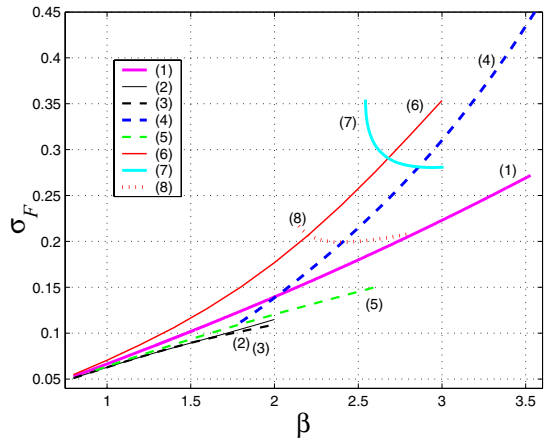

(b)

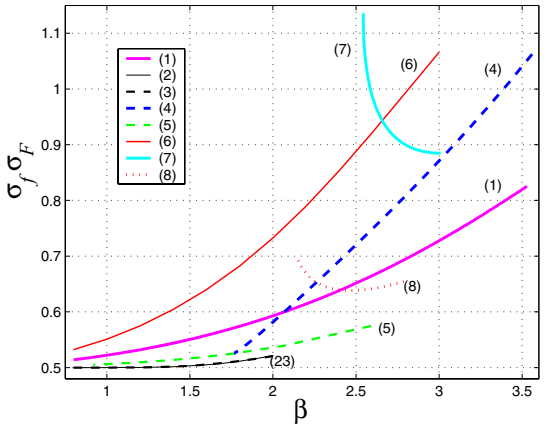

(c)

Figure 15. Uncertainty principle for the quadrature pairs for $\lambda_0 = 20$. Cauchy filters (solid Magenta curves (1)), Gabor with Ronse zero DC correction using $\tilde{\sigma} = \sigma$ (solid Black curves (2)) and $\tilde{\sigma} = \check{\sigma}$ (dashed Black curves (3)), DoG filters (dashed Blue curves (4)), Gaussian derivative filters (dashed Green curves (5)), log-Gabor (solid Red curves (6)) and Sarkar and Boyer filters for best $\Gamma\Sigma$ (i.e Deriche filter) (solid Cyan curves (7)) and best $\Gamma\Sigma\Omega_S$ (dots Red curves (8)).

Sarkar and Boyer family is opposite to the dependence of other families. This result is expected as, for example, we already pointed out that the Deriche family has more aliasing for smaller bandwidths. This is because the bandwidth is inversely proportional to the order a of the derivative of the smoothing function and the decay of its Fourier transform is of order $\omega^{(a-4)}$. Notice that the Sarkar and Boyer filter has a far better frequency localisation than the Deriche one, especially for smaller bandwidths.

The relative behaviour of the different families regarding the uncertainty principle shown in Fig. 15(c) is similar to their relative behaviour regarding σ_F. The zero DC corrected Gabor filter is close to the limit ($\frac{1}{2}$) almost everywhere, followed by the Gaussian derivatives filter. Because of their tailed nature, the log-Gabor wavelets are the farthest from the limit with the Deriche filter for $2.54 < \beta < 2.66$ (i.e $a \in [1.46, 2]$); the Sarkar and Boyer filters seems to have the best scale-space localisation for $2.5902 < \beta \leq 2.7875$ (basically for a bandwidth greater than the 1st derivative of a Gaussian until the bandwidth of Sarkar and Boyer's edge operator). For very large bandwidths, Cauchy kernels are the closest to the limit.

In the case of feature detection we can locate Canny's, Deriche and Sarkar and Boyer's edge operators as well as Ziou's line detector on these curves (Fig. 15, curves (5), (7), (8) and (7) respectively); these operators are optimal in the sense of Canny's criteria. This gives some insight on the performance of the other families, in the sense of Canny. Recently, the log-Gabor filters have been proposed as the choice of quadrature pair for feature detection. Spatial localisation of the filters is of great interest. On inspection of Fig. 15(a), we notice that the DoG filter has better spatial localisation than log-Gabors for a bandwidth greater than 2.1 octave and the Sarkar and Boyer filters are far better in their range of definition. When $\beta < 2$ log-Gabors are better than the DoG but the Cauchy filter has a comparative localisation. Fig. 15(b) shows that the DoG and the Cauchy family have always a better frequency localisation than log-Gabor kernels and Fig. 15(c) shows that the two families have a better uncertainty principle than the log-Gabor family. All three families are invariant to a grey level shift and to an additive ramp. Finally, note that the Deriche edge operator is closer to the DoG filter, and the Sarkar and Boyer edge operator is closer to the Cauchy family. Hence, for edge detection log-Gabor kernels are not the best choice.

However, for line detection, log-Gabor filters can have good performance as they are the closest to Ziou's optimal line detector. However, we found that the DoG filter for larger bandwidths has similar performance to the Ziou line detector. In addition Ziou's line detector has poor spectral localisation and the largest aliasing.

Our results suggests that the DoG filter is the best to use for combined line and edge detection. The Cauchy family is an interesting alternative, and we have the analytical expressions of the filters in the spatial and the frequency domain. Further experiments are needed to investigate their use in more detail.

4. Concluding Remarks

We began by stressing the importance of phase information in computer vision, then provided the reader with a short summary of the definition of the local phase in one dimension, and its extension to multi-dimensional signals. In practice, the estimation of the local phase and the related quantity, local energy, uses a pair of band-pass quadrature filters. Several families of quadrature pairs have been proposed and applied in the literature, in a number of different applications. Most authors have not provided a reasonable justification for the use of a particular family apart from simplicity of use or the satisfaction of the zero DC condition. This is particularly the case in feature detection where, for example, several authors have not considered the invariance of the filters to an additive ramp (smooth gradient). This property is desirable and has been noted in classical feature detection (see e.g. [7]). Our analysis attempts to put the justification on a sound foundation.

Specifically, in the paper, we have studied mathematically the most common quadrature filters in the literature. We have provided either a mathematical expression or a numerical estimation for most filter properties. Key results and properties are summarised in Table 3.

In the case of feature detection, we presented the first attempt to use classical edge/line operators for the design of a quadrature pair. Although the main advantage of phase-based feature detection is that it is a unified detection approach (not only for edges or lines), we can learn a lot from the separate behaviour of the even part (symmetric detector, lines for example) and the odd part (asymmetric detector, edges for example). Interestingly, we found that most of the classical optimal operators, have large bandwidth and several

authors point out that broad bandwidth filters have a better SNR in phase-based detection.

Our analysis shows that Gabor filters are not a good choice for feature detection. The odd part has poor performance in the sense of Canny in comparison to the 1st derivative of a Gaussian, to Sarkar and Boyer filter and to the Deriche filter; and the even part does not satisfy the zero DC correction and hence needs correction. The zero DC correction is possible but the filters are still not truly in quadrature, except if the negative frequencies are zeroed in the case of a Fourier domain implementation. Gabor filters are sensitive to smooth gradients.

We also concluded that log-Gabor kernels are not a very good choice for feature detection. As we showed, the DoG family and the Cauchy family have better properties. The Sarkar and Boyer's filter has very good properties, for example for a bandwidth close to 2 octaves, this family has very good spatial localisation. In the case that we are interested only in one type of features (edges or lines), a natural choice is to use the Sarkar and Boyer family which is optimal in the sense of Canny.

Regarding the use of quadrature filters for velocity estimation, we showed that all the families have similar behaviours for small bandwidths (in terms of phase linearity and phase stability). The zero DC corrected Gabor filters could be used. If we want to be invariant to a smooth gradient (in the case where the conservation criteria is violated), the Gaussian derivative family would be a natural choice as they have close behaviour to the Gabor filters in terms of phase stability and the uncertainty principle. The disadvantage of using the Gaussian derivative filter is the loss of the spatial representation of the filters. In this case, the Cauchy family offers an alternative and has the advantage of being invariant to smooth gradients and having analytical expression in the spatial and the Fourier domain.

Appendix A: Phase Stability Given White Gaussian Noise

The stability of phase can be measured in terms of the differences in phase response between two arbitrary neighbouring scale-space locations, $\mathbf{p}_0 = (x_0, \lambda_0)$, $\mathbf{p}_1 = (x_1, \lambda_1)$. We denote the filter response to the input $f(x)$ at scale-space position $\mathbf{p}_j$ by:

$$g_j = h(x - x_j, \lambda_j) \circledast f(x) = \langle h(x_j - x, \lambda_j),\ f(x) \rangle, \tag{A.1}$$

where $\langle f(x),\ g(x) \rangle = \int_{-\infty}^{\infty} f(x)^{\star}\, g(x)\, dx$ is the inner product.

The phase differences, as a function of the relative scale-space position, $\mathbf{p}_1 - \mathbf{p}_0 = (\Delta x,\ \Delta\lambda)$ can be written as:

$$\Delta\phi = \arg[g_1] - \arg[g_0]. \tag{A.2}$$

Phase is perfectly stable when $\Delta\phi$ is constant with respect to changes in scale $\Delta\lambda$; and it is linear with respect to spatial position when $\Delta\phi$ is linear function of Δx.

To characterise the stability of phase behaviour through scale-space, Fleet and Jepson [24] examined the response of the filter kernel, $h(x, \lambda)$ and its phase behaviour to stationary, zero mean white Gaussian noise. The authors derived an approximation to the mean phase difference $E[\Delta\phi]$, and an upper bound of the mean variation about the mean $E[|\Delta\phi - E[\Delta\phi]|]$. Given the above noise assumptions:

$$E[\Delta\phi] \approx \mu(z) = \arg[z] \tag{A.3}$$

$$E[|\Delta\phi - E[\Delta\phi]|] \leq b(z) = \frac{\sqrt{1 - |z|^2}}{|z|}, \tag{A.4}$$

where the complex scalar z is a function of scale-space position and is given by:

$$\begin{aligned} z(\mathbf{p}_1 - \mathbf{p}_0) &= z(\Delta x,\ \Delta\lambda) \\ &= \langle h(x_0 - x, \lambda_0),\ h(x_1 - x,\ \lambda_1) \rangle, \end{aligned} \tag{A.5}$$

where the kernel h has to satisfy the two following conditions:

(1) Normalisation condition:

$$\|h(x,\ \lambda)\| = \langle h(x, \lambda), h(x, \lambda) \rangle = 1. \tag{A.6}$$

(2) Translational invariance and self-similarity across scales (i.e their octave bandwidth remains constant, independent of the scale to which they are tuned):

$$h(x,\ \lambda) = \frac{1}{\sqrt{\lambda}}\, h(x/\lambda,\ 1). \tag{A.7}$$

Appendix B: Optimal Linear Edge Detector Criteria

Consider the problem of detecting an ideal feature (edge or line) $f_F(x)$, centred at $x = 0$ using an

observation corrupted by an additive white Gaussian noise with standard deviation $\sigma = 1$. Canny [7, 8] was the first to formulate the detection problem for a linear edge detector $f_O(x)$ as an optimisation problem. As Canny pointed out, the key to the design of an effective edge operator is accurate evaluation of its performance. Canny defined three different criteria to be maximised:

Good Detection: Given the white Gaussian noise assumption, the probability of false detection decreases with increasing the signal-to-noise ratio $\Sigma(f)$ given by:

$$\Sigma(f_O) = \frac{|f_F(x) \circledast f_O(x)|}{\sqrt{\int_{-\infty}^{\infty} f_O^2(x)\,dx}} = \frac{\left|\int_{-\infty}^{\infty} f_F(-x) f_O(x)\,dx\right|}{\sqrt{\int_{-\infty}^{\infty} f_O^2(x)\,dx}}. \tag{B.1}$$

Good Localisation: This second criterion is defined as the variance of the maximum of the filter response about the correct location.[9] Canny used an approximation based on a Taylor's expansion of the filter output:[10]

$$\text{for edges} \quad \Lambda(f_O) = \frac{\left|\int_{-\infty}^{\infty} f_F'(-x) f_O'(x)\,dx\right|}{\sqrt{\int_{-\infty}^{\infty} {f_O'}^2\,dx}}. \tag{B.2}$$

$$\text{for lines} \quad \Lambda(f_O) = \frac{\left|\int_{-\infty}^{\infty} f_F(-x) f_O''(x)\,dx\right|}{\sqrt{\int_{-\infty}^{\infty} {f_O'}^2 dx}}. \tag{B.3}$$

Low Number of Multiple Responses: This criterion was designed to minimise the number of spurious maxima within the operator spatial spread [8]:

$$\Omega_C(f_O) = 2\pi \sqrt{\frac{\int_{-W}^{W} {f_O'}^2 dx}{\int_{-W}^{W} {f_O''}^2 dx}} = kW, \tag{B.4}$$

where W is the operator width and k is a positive constant.

Sarkar and Boyer [67] point out that the above multiple response criteria must be modified to be applied to IIR filters. In other words we should provide an estimate of the operator width Sarkar and Boyer [67] defined the width of the filter as the normalised root mean square deviation of the function $f_O^2(x)$ from the origin.

$$\bar{W} = \sqrt{\frac{\int_{-\infty}^{\infty} x^2 f_O^2(x)\,dx}{\int_{-\infty}^{\infty} f_O^2(x)\,dx}}. \tag{B.5}$$

Hence, they proposed a new expression for $\Omega(f)$:

$$\Omega_S(f_O) = 2\pi \sqrt{\frac{\int_{-\infty}^{\infty} {f_O'}^2\,dx}{\int_{-\infty}^{\infty} {f_O''}^2\,dx}} \sqrt{\frac{\int_{-\infty}^{\infty} f_O^2(x)\,dx}{\int_{-\infty}^{\infty} x^2 f_O^2(x)\,dx}}, \tag{B.6}$$

Then, the optimality of the detector is defined with respect to the maximisation of the following quantity [8]:

$$C_c(f_O) = \Gamma(f_O)\,\Sigma(f_O)\,\Omega(f_O). \tag{B.7}$$

For an ideal step edge (B.7) is given by:

$$C_c(f_O) = \frac{\left|\int_{-\infty}^{0} f_O(x)\,dx\right| |f_O'(0)|}{\sqrt{\int_{-\infty}^{\infty} f_O^2(x)\,dx \int_{-\infty}^{\infty} {f_O''}^2\,dx}}. \tag{B.8}$$

Acknowledgments

This work was funded by the EC project ADEQUATE (IST: 1999-10837) and the UK EPSRC funded IRC in Medical Image Analysis and Signals (MIAS).

Notes

1. Throughout, we mean "local" or "instantaneous" ... When 1-D signals are discussed, the "space" variable may be called "time".
2. Throughout, we use the following convention: if $f(x)$ is a 1D function then $F(\omega)$ is its Fourier transform.
3. Normally, energy is define as the amplitude-squared [26, 65], however, some authors (see for e.g. [40, 57, 64]), define the energy as being the amplitude.
4. Of course, this is not an exhaustive list of quadrature filters in the literature. We did not include, for example, *shiftable* [70] filters as this property implies their use in a multiscale framework as well as the robust quadrature filters proposed in [54].
5. Note: the use of these two normalisation conditions is a recurrent theme throughout.
6. Strictly speaking, log-Gabor filters are invariant to an additive polynomial function of order $n < \infty$.
7. Mathematically, the 2nd derivative of a Gaussian is well approximated by the DoG filter when $\sigma' \to \sigma$. However, the DoG filter preferred by Marr and Hildreth [53] is for $\sigma = 1.6\sigma'$.

8. Of course the optimality is debatable as for example we found that the even DoG filter (when $\gamma \leq 0.05$) has better performance than Ziou's line detector, in the sense of Canny, using the following line model: $F(x) = \text{rect}((x - 0.25)/0.5)$.
9. Although the agreement [5, 67] and the disagreement [73], this is the most popular localisation measure in this context.
10. The Taylor expansion of the filters output are different for an edge detector and a line detector because the edge detector is odd and the line detector is even. See Canny [8] for the details.

References

1. T. Aach, A. Kaup, and R. Mester, "On texture analysis: Local energy transforms versus quadrature filters," *Signal Processing*, Vol. 45, pp. 173–181, 1995.
2. J.L. Barron, D.J. Fleet, and S.S. Beauchemin, "Performance of optical flow techniques," *Int. J. Computer Vision*, Vol. 12, pp. 43–77, 1994.
3. D. Boukerroui, J.A. Noble, and M. Brady, "On Gabor zero DC correction," Technical Report, MVL, Oxford University, 2002. http://www.robots.ox.ac.uk/∼djamal/.
4. A.C. Bovik, M. Clark, and W.S. Geisler, "Multichannel texture analysis using localized spatial filters," *IEEE Trans. PAMI*, Vol. 12, No. 1, pp. 55–73, 1990.
5. K.L. Boyer and S. Sarkar, "On the localisation performance measures and optimal edge detection," *IEEE Trans. PAMI*, Vol. 16, No. 1, pp. 106–108, 1994.
6. T. Bülow, "Hypercomplex spectral signal representations for the processing and analysis of images," Ph.D. dissertation, Christian Albrechts, Univ., Keil, Germany, 1999.
7. J.F. Canny, "Finding edges and lines in images," MIT Artif. Intell. Lab., Massachusetts Inst. Technol., Cambridge, MA, A.I. Memo 720, 1983.
8. J.F. Canny, "A computational approach to edge detection," *IEEE Trans. PAMI*, Vol. 8, pp. 679–714, 1986.
9. D. Casasent and J.S. Smokelin, "Real, imaginary, and clutter Gabor filter fusion for detection with reduced false alarms," *Optical Engineering*, vol. 33, pp. 2255–2263, 1994.
10. C-.M. Chen, H.H.-S. Lu, and K.-C. Han, "A textural approach based on Gabor functions for texture edge detection in ultrasound images," *Ultrasound in Med. & Biol.*, Vol. 27, No. 4, pp. 515–534, 2001.
11. R.M. Corless, G.H. Gonnet, D.E.G. Hare, D.E Jeffrey, and D.E. Knuth, "On the Lambert W function," *Advances in Computational Mathematics*, Vol. 5, pp. 329–359, 1996. http://pineapple.apmaths.uwo.ca/∼rmc/papers/LambertW/index.html.
12. J.G Daugman, "Two-dimensional spectral analysis of cortical receptive field profiles," *Vision Research*, Vol. 10, pp. 847–856, 1980.
13. R. Deriche, "Optimal edge detection using recursive filtering," in *Proc. Int. Conf. Computer Vision*, London, UK, 1987, pp. 167–187.
14. R. Deriche, "Fast algorithms for low-level vision," *IEEE Trans. PAMI*, Vol. 12, No. 1, pp. 78–86, 1990.
15. D. Dunn and W.E. Higgins, "Optimal Gabor filters for texture segmentation," *IEEE Trans. Image Processing*, Vol. 4, No. 7, pp. 947–964, 1995.
16. M. Elad, P. Teo, and Y. Hel-Or, "Optimal filters for gradient-based motion estimation," in *Proc. Int. Conf. Computer Vision*, Corfu, Greece, 1999, pp. 559–565.
17. I.H. Elder and S.W. Zucker, "Local scale control for edge detection and blur estimation," *IEEE Trans. PAMI*, Vol. 20, No. 7, pp. 699–716, 1998.
18. M. Felsberg and G. Sommer, "A new extension of linear signal processing for estimating local properties and detecting features," *DAGM Symposium Mustererkennung*, Kiel, Germany, 2000, pp. 195–202.
19. M. Felsberg and G. Sommer, "The multidimensional isotropic generalisation of quadrature filters in geometric algebra," in *Proc. Int. Workshop on Algebraic Frames for the Perception-Action Cycle*, Kiel, Germany, 2000, pp. 175–185.
20. M. Felsberg and G. Sommer, "The monogenic signal," *IEEE Trans. Signal Processing*, Vol. 49, No. 12, pp. 3136–3144, 2001.
21. M. Felsberg and G. Sommer, "Scale adaptive filtering derived from the Laplace equation," in *Lecture Notes in Computer Science, 23rd DAGM Symp. Mustererken-nung*, 2191, B. Radig and S. Florczyk (Eds.), Heidelberg, Germany, 2001.
22. D.J. Field, "Relations between the statistics of natural images and the response properties of cortical cells," *J. Opt. Soc. Am.*, Vol. A, No. 4, pp. 2379–2394, 1987.
23. D.J. Fleet and A.D. Jepson, "Computational of component image velocity from local phase information," *Int. J. Computer Vision*, Vol. 5, pp. 77–104, 1990.
24. D.J. Fleet and A.D. Jepson, "Stability of phase information," *IEEE Trans. PAMI*, Vol. 15, No. 12, pp. 1253–1268, 1993.
25. W.T. Freeman and D. Adam, "The design and the use of steerable filters," *IEEE Trans. PAMI*, Vol. 13, No. 9, pp. 891–906, 1991.
26. D. Gabor, "Theory of communication," *J. IEE*, Vol. 93, pp. 429–457, 1946.
27. G.H. Granlund and H. Knutsson, *Signal Processing for Computer Vision,* Kluwer Academic Publishers: Dordrecht, 1995.
28. S.L. Hahn, *Hilbert Transform in Signal Processing*, Artech House: Boston, MA 1996.
29. E.R. Hancock, "Resolving edge-line ambiguities using probabilistic relaxation," in *Proc. IEEE Computer Vision and Pattern Recognition Conference*, 1993, pp. 300–306.
30. F. Heitger, L. Rosenthaler, R. von der Heydt, E. Peterhans, and O. Kübler, "Simulation of neural contour mechanisms: From simple to the end-stopped cells," *Vision Research*, Vol. 32, pp. 963–981, 1992.
31. F. Heitger, "Feature detection using suppression and enhancement," Tech. Rep., Image Science Lab, ETH-Zurich, Switzerland, NR. 163, 1995.
32. R. Highnam and M. Brady, *Mammographic Image Analysis*, Kluwer, 1999.
33. C.-L. Huang and Y.-T. Chen, "Motion estimation method using a 3D steerable filter," *Image and Vision Computing*, Vol. 13, No. 1, pp. 21–32, 1995.
34. M. Idrissa and M. Acheroy, "Texture classification using Gabor filters," *Pattern Recognition Letters*, Vol. 23, pp. 1095–1102, 2002.
35. A.K. Jain and F. Farrokhnia, "Unsupervised texture segmentation using Gabor filters," *Pattern Recognition*, Vol. 23, No. 12, pp. 1167–1186, 1991.
36. A.D. Jepson and M. Jenkin, "Fast computation of disparity from phase differences," in *Proc. IEEE Computer Vision and Pattern Recognition Conference*, San Diego, 1989, pp. 398–403.

37. L.M. Kennedy and M. Basu, "A Gaussian derivative operator for authentic edge detection and accurate edge localization," *Int. J. Pattern Recognition and Artificial Intelligence*, Vol. 13, pp. 367–380, 1999.
38. S.A. Klein and D.M. Levi, "Hyperacuity thresholds of 1 sec: Theoretical predictions and empirical validation," *J. Opt. Soc. Am.*, Ser. *A*, Vol. 2, No. 7, pp. 1170–1190, 1985.
39. A.K. Klein, F. Lee, and A.A. Amini, "Quantitative coronary angiography with deformable spline models," *IEEE Trans. Medical Imaging*, Vol. 16, No. 5, pp. 468–482, 1997.
40. P. Kovesi, "Image feature from phase congurency," *Videre: Journal of Computer Vision Research*, Vol. 1, No. 3, pp. 1–26, 1999.
41. P. Kruizinga and N. Petkov, "Nonlinear operator for oriented texture," *IEEE Trans. Image Processing*, Vol. 8, No. 10, pp. 1395–1407, 1999.
42. P. Kruizinga and N. Petkov, "Nonlinear operator for blob texture segmentation," in *Proc. NSIP'99, IEEE Workshop on Nonlinear Signal Processing*, II, A.S. Cetin, et al. (Eds.), Antalya, Turkey, 1999, pp. 881–885.
43. P. Kruizinga, N. Petkov, and S.E. Grigorescu, "Comparison of texture features based on Gabor filters," in *Proc. of the 10th International Conference on Image Analysis and Processing*, Venice, Italy, 1999, pp. 142–147.
44. C. Kuglin and D. Hine, "The phase correlation image alignment method," *IEEE Int. Conf. Cybern. Society*, 1975, pp. 163–165.
45. K.G. Larkin, D.J. Bone, and M.A. Oldfield, "Natural demodulation of two-dimensional fringe patterns: I. General background of the spiral phase quadrature transform," *J. Opt. Soc. Am. A*, Vol. 18, No. 8, pp. 1862–1870, 2001.
46. T.S. Lee, "Image representation using 2D Gabor wavelets," *IEEE Trans. PAMI*, Vol. 18, No. 10, pp. 959–971, 1996.
47. J.A.F. Leite and E.R. Hancock, "Statistically combining and refining multichannel information," in *Progress in Image Analysis and Processing III*, S. Impedovo (Ed.), World Scientific, 1994, pp. 193–200.
48. J. Little, "Accurate early detection of discontinuities," *Vision Interface*, pp. 97–102, 1992.
49. H. Liu, T.-H. Hong, M. Herman, and R. Chellappa, "A general motion model and spatio-temporal filters for computing optical flow," *Int. J. Computer Vision*, Vol. 22, No. 2, pp. 141–172, 1997.
50. D.G. Lowe, "Object recognition from local scale-invariant features," in *Proc. Int. Conf. Computer Vision*, 2, Corfu, Greece, 1999, pp. 1150–1157.
51. S. Mallat, *A Wavelet Tour of Signal Processing*, Academic Press, 1999.
52. S. Marčelja, "Mathematical description of the responses of simple cortical cells," *J. Opt. Soc. Am.*, Vol. 70, pp. 1297–1300, 1980.
53. D. Marr and E. Hildreth, "Theory of edge detection," *Proc. Royal Society London*, Vol. B207, pp. 187–217, 1980.
54. J.L. Marroquin, J.E. Figueroa, and M. Servin, "Robust quadrature filters," *J. Opt. Soc. Am. A*, Vol. 14, No. 4, pp. 779–791, 1997.
55. K. Mikolajczyk and C. Schmid, "Indexing based on scale invariant interest points," in *Proc. Int. Conf. Computer Vision*, 1, Vancouver, Canada, 2001, pp. 525–531.
56. M.C. Morrone and R.A. Owens, "'Feature detection from local energy," *Pattern Recognition Letters*, Vol. 6, pp. 301–313, 1987.
57. M.C. Morrone, A. Navangione, and D. Burr, "An adaptive approach to scale selection for line and edge detection," *Pattern Recognition Letters*, Vol. 16, pp. 667–677, 1995.
58. M. Mulet-Parada and J.A. Noble, "2D + T acoustic boundary detection in echocardiography," *Medical Image Analysis*, Vol. 4, pp. 21–30, 2000.
59. K. Okajima, "The Gabor function extracts the maximum information from input local signals," *Neural Networks*, Vol. 11, pp. 435–439, 1998.
60. K. Okajima, "Two-dimensional Gabor-type receptive field as derived by mutual information maximization," *Neural Networks*, Vol. 11, pp. 441–447, 1998.
61. D. Reisfeld, "The constrained phase congruency feature detector: Simultaneous localisation, classification and scale determination," *Pattern Recognition Letters*, Vol. 17, pp. 1161–1169, 1996.
62. N. Petkov and P. Kruizinga, "Computational models of visual neurons specialised in the detection of periodic and aperiodic oriented visual stimuli: Bar and grating cells," *Biological Cybernetics*, Vol. 76, No. 2, pp. 83–96, 1997.
63. T. Poggio, H. Voorhees, and A. Yuille, "A regularised solution to edge detection," MIT Artif. Intell. Lab., Massachusetts Inst. Technol., Cambridge, MA, A.I. Memo 833, 1985.
64. B. Robbins and R. Owens, "2D feature detection via local energy," *Image and Vision Computing*, Vol. 15, pp. 353–368, 1997.
65. C. Ronse, "On idempotence and related requirements in edge detection," *IEEE Trans. PAMI*, Vol. 15, No. 5, pp. 484–491, 1993.
66. C. Ronse, "The phase congruence model for edge detection in two-dimensional pictures: A mathematical study," Tech. Rep., Rap95-11, Université de Strasbourg, LSIIT-URA 1871, 1995.
67. S. Sarkar and K.L. Boyer, "On optimal infinite impulse response edge detection filters," *IEEE Trans. PAMI*, Vol. 13, No. 11, pp. 1154–1171, 1991.
68. J. Shen and S. Castan, "An optimal linear operator for edge detection," in *Proc. IEEE Computer Vision and Pattern Recognition Conference*, June, Miami, FL, 1986, pp. 109–114.
69. J. Shen and S. Castan, "An optimal linear operator for step edge detection," *CVGIP: Graphical Models and Image Processing*, Vol. 54, No. 2, pp. 112–133, 1992.
70. E.P. Simoncelli, W.T. Freeman, E.H. Adelson, and D.J. Heeger, "Shiftable multiscale transforms," *IEEE Trans. Information Theory, Special Issue on Wavelets*, Vol. 38, No. 2, pp. 587–607, 1992.
71. E.P. Simoncelli, "Design of multi-dimensional derivative filters," in *Proc. IEEE Int. Conf. Image Processing*, Austin, Texas, 1994, pp. 790–794.
72. E.P. Simoncelli and H. Farid, "Steerable wedge filters for local orientation analysis," *IEEE Trans. Image Processing*, Vol. 5, No. 9, pp. 1377–1382, 1996.
73. H.D. Tagare and J.P. deFigueiredo, Reply to "On the localisation performance measure and optimal edge detection," *IEEE Trans. PAMI*, Vol. 16, No. 1, pp. 108–110, 1994.
74. S. Venkatesh and R. Owens, "On the classification of image features," *Pattern Recognition Letters*, Vol. 11, pp. 339–349, 1990.
75. T.P. Weldon, W.E. Higgins, and D.F. Dunn, "Gabor filter design for multiple texture segmentation," *Optical Engineering*, Vol. 35, No. 10, pp. 2852–2863, 1996.
76. T.P. Weldon and W.E. Higgins, "An algorithm for designing multiple Gabor filters for segmenting multi-textured images," in *Proc. IEEE Int. Conf. Image Processing*, Chicago, IL, 1998.

77. L. Wiskott, "Segmentation from motion: combining Gabor- and Mallat-wavelets to overcome the aperture and correspondance problems," *Pattern Recognition*, Vol. 32, pp. 1751–1766, 1999.
78. D. Ziou, "Line detection using an optimal IIR filter," *Pattern Recognition*, Vol. 24, No. 6, pp. 465–478, 1991.
79. D. Ziou and S. Tabbone, "Edge detection techniques: An overview," *Pattern Recognition and Information Analysis*, Vol. 8, pp. 537–554, 1998.
80. D. Ziou, "Finding lines in grey-level images," Tech. Rep., N. 240. Université de Sherbrooke, 1999.

Djamal Boukerroui was borne in Bejaïa (Algeria) in 1972. He received the B.S. degree in 1990, and the M.S. degree in electronics in July 1995 form ENP of Algiers (Algeria). He received the Ph.D degree in Image Processing at CREATIS Laboratory of INSA of Lyon (France) in 2000. From March 2000 to August 2002 he was a Research Assistant at the Medical Vision Laboratory, Department of Engineering Science, University of Oxford where he worked on the analysis of echocardiographic image sequences. Since September 2002, he joined the Department of Information Processing Engineering of Compiègne University of Technology as Maître de Conférences, and he is a member of HEUDIASYC [research unit associated with CNRS (#6599)]. His future research will include, Features extraction, optical flow estimation and Content Based Medical Image Retrieval.

J. Alison Noble D. Phil (Oxon), MA (Oxon), FIEE Professor Alison Noble has 16 years of research experience in image analysis, including 5 years in industry, and has been a faculty member at the University of Oxford for 8 years. Her current main research interests are in low level vision, and specifically its application in ultrasound image analysis and in-vivo soft tissue analysis (of the heart and breast). She has 27 journal publications in computer vision and its application in manufacturing and medicine, around 75 other publications presented at conferences, 3 patents (2 US, 1 UK) and three further UK patents pending. She is on the Editorial Advisory Boards of Medical Image Analysis (Elsevier) and Ultrasound in Medicine and Biology (Elsevier) journals, is a regular reviewer for a number of other journals and international conferences in her research field, and is Co-Chair of the 18th International Conference on Information Processing in Medical Imaging to be held in Ambleside, UK, in 2003.

Michael Brady FRS, FREng BP Professor of Information Engineering at the University of Oxford. Professor Brady's degrees are in mathematics (BSc and MSc from Manchester University, and PhD from the Australian National University). At Manchester University, he was awarded the Renold Prize as the outstanding undergraduate of his year. Professor Brady combines his work at Oxford University, where he founded the Robotics Laboratory and the Medical Vision Laboratory (MVL), with a range of entrepreneurial activities. He is Director of the EPSRC/MRC Inter-disciplinary research consortium on From Medical Images and Signals to Clinical Information (The IRC involves Oxford University, UCL, King's College London (including Guy' s Hospital), and the University of Manchester. It also involves clinicians from over 30 specialities and is supported by over 20 companies. The chair of the Industrial Advisory Group will be Professor Will Stewart FREng, who is also a member of the Advisory Panel of the Department of Engineering Science.) He was appointed Senior Research Scientist of the MIT Artificial Intelligence Laboratory in 1980, and helped found its world famous robotics laboratory. In 1985, he left MIT to take up a newly created Professorship in Information Engineering. Professor Brady serves as a non-executive director and Deputy Chairman of Oxford Instruments plc, as a non-executive director of AEA Technology, and, until recently, Isis Innovation (Oxford University's intellectual property company). Professor Brady is a founding Director of the start-up companies Guidance and Control Systems and Mirada Solutions.

Professor Brady is the author of over 275 articles in computer vision, robotics, medical image analysis, and artificial intelligence, and the author or editor of nine books, including: Robot Motion (MIT Press, 1984), Robotics Science (MIT Press, 1989), Robotics Research (MIT Press 1984), and Mammographic Image Analysis (Kluwer, January 1999). He was Editor of the Artificial Intelligence Journal (1987–2002), and founding Editor of the International Journal of Robotics Research (1981–2000). He is a member of the Editorial Board of fourteen journals, most recently Medical Image Analysis.

Professor Brady was elected a Fellow of the Royal Academy of Engineering (UK) in 1991 and a Fellow of the Royal Society (UK) in 1997. He is a Fellow of the Institution of Electrical Engineers and a founding Fellow of the Association of Artificial Intelligence, and a Fellow of the Institute of Physics. He is a member of the Conseil Scientifique de l'INRIA France. He has been awarded honorary doctorates by the universities of Essex, Manchester, Liverpool, Southampton, and Paul Sabatier (Toulouse). He was awarded the IEE Faraday Medal for 2000 and the IEEE Third Millennium Medal for the UK.